ACS OMEGA

http://pubs.acs.org/journal/acsodf

Article

# Destruction of Cell Topography, Morphology, Membrane, Inhibition of Respiration, Biofilm Formation, and Bioactive Molecule Production by Nanoparticles of Ag, ZnO, CuO, $TiO_2$, and $Al_2O_3$ toward Beneficial Soil Bacteria

Bilal Ahmed,* Fuad Ameen, Asfa Rizvi, Khursheed Ali, Hana Sonbol, Almas Zaidi, Mohammad Saghir Khan, and Javed Musarrat

Cite This: *ACS Omega* 2020, 5, 7861−7876

Read Online

ACCESS | Metrics & More | Article Recommendations | Supporting Information

**ABSTRACT:** The unregulated discharge of nanoparticles (NPs) from various nanotechnology industries into the environment is expected to alter the composition and physiological functions of soil microbiota. Considering this knowledge gap, the impact of five NPs (Ag, ZnO, CuO, $Al_2O_3$, and $TiO_2$) differing in size and morphology on growth behavior and physiological activity of *Azotobacter chroococcum*, *Bacillus thuringiensis*, *Pseudomonas mosselii*, and *Sinorhizobium meliloti* were investigated. Various biochemical and microscopic approaches were adopted. Interestingly, all bacterial strains were found sensitive to Ag-NPs and ZnO-NPs but showed tolerance toward CuO, $Al_2O_3$, and $TiO_2$-NPs. The loss of cellular respiration due to NPs was coupled with a reduction in population size. ZnO-NPs at 387.5 $\mu g\ mL^{-1}$ had a maximum inhibitory impact on *A. chroococcum* and reduced its population by 72%. Under Ag-NP stress, the reduction in IAA secretion by bacterial strains followed the order *S. meliloti* (74%) > *P. mosselii* (63%) > *A. chroococcum* (49%). The surface of bacterial cells had small- or large-sized aggregates of NPs. Also, numerous gaps, pits, fragmented, and disorganized cell envelopes were visible. Additionally, a treated cell surface appeared corrugated with depressions and alteration in cell length and a strong heterogeneity was noticed under atomic force microscopy (AFM). For instance, NPs induced cell roughness for *P. mosselii* followed the order 12.6 nm (control) > 58 nm (Ag-NPs) > 41 nm (ZnO-NPs). TEM analysis showed aberrant morphology, cracking, and disruption of the cell envelope with extracellular electron-dense materials. Increased permeability of the inner cell membrane caused cell death and lowered EPS production. Ag-NPs and ZnO-NPs also disrupted the surface adhering ability of bacteria, which varied with time and concentration of NPs. Conclusively, a plausible mechanism of NP toxicity to bacteria has been proposed to understand the mechanistic basis of ecological interaction between NPs and resourceful bacteria. These results also emphasize to develop strategies for the safe disposal of NPs.

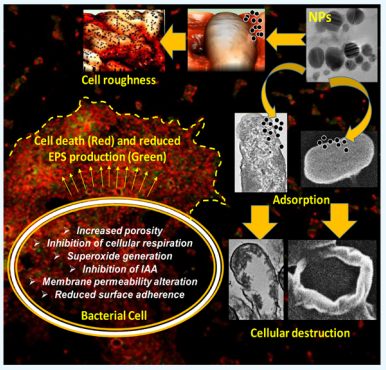


## INTRODUCTION

Nanoparticles (NPs) generally defined as the particles ranging in size between 1 and 100 nm with multiple properties such as an extremely high surface-to-volume ratio, and specific surface area[1,2] NPs are being used in areas like agriculture, biomedical, pharmaceuticals, electronics, defense, and aerospace industries.[3−5] Among NPs, the production of metal and metal oxide NPs (MONPs) due to their wide range of end uses are likely to enhance their probability to enter the environment during the production, use, and disposal. The NPs emerging from sources like industries, sewage wastes, wastewater treatment plants, tannery effluents, and other metal discharging industries are the major cause of nanopollution that adds considerable amounts of NPs to the terrestrial environment.[6,7] As per one estimate, up to 28% of total NPs production is expected to enter into terrestrial soils.[8] For instance, the consumption of silver (Ag) NPs and zinc oxide (ZnO) NPs in Europe per capita and their release has been significant, which is broadly distributed in the European territory.[9] Additionally, NPs are rendered susceptible to environmental conditions when released and can alter their oxidation state, aggregation, precipitation, etc.[10] There are, however, serious concerns over the use of NPs due to their deleterious but variable impact on environmental sustainability.[11,12] Following deposition in soils, NPs either alone or synergistically affect the composition and functions of soil microbiota,[13,14] the fertility of soils,[15] and via food chain, they affect human health.[16]

Soil microorganisms play key roles in immobilization/cycling of nutrients/carbon and detoxification/degradation of

Received: December 1, 2019
Accepted: March 23, 2020
Published: April 1, 2020

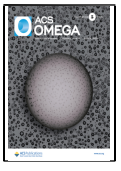

Table 1. Morphological Characteristics of Reference Bacterial Strains

| | colony characteristics | | | | |
|---|---|---|---|---|---|
| isolate designation | pigmentation | shape | average size (mm) | margin | growth medium |
| *B. thuringiensis* | white | irregular | 6.8 | wavy | nutrient agar |
| *P. mosselii* | creamy white | circular | 1.15 | smooth | nutrient agar |
| *S. meliloti* | light pink | round | 1.26 | regular | YEM agar[a] |
| *A. chroococcum* | dark brown | irregular | 10.27 | wavy | AM agar[b] |

[a]YEM, yeast extract mannitol [b]AM, Ashby's mannitol

contaminants, leading eventually to enhanced soil health.[17] Among variously distributed heterotrophic microflora, bacterial populations belonging to different species form about 15% of the total microbial populations[18] and directly or indirectly improve the plant growth.[19] The NPs are reported to inhibit bacterial growth[20] due to the release of metal ions from NPs[21] and manifest toxicity via generation of reactive oxygen species (ROS), such as superoxide anions.[22] Given the importance of plant growth-promoting rhizobacteria (PGPR) to plant health, the interactions of NPs-PGPR are crucial.[23] Similar to the other xenobiotics, the negative effect of NPs on soil beneficial microbes is gradually increasing and still not well understood. In this regard, the direct entry of Fe-NPs and $TiO_2$-NPs used in environmental remediation and water treatment has been found to inhibit and stimulate the growth of target organisms,[24,25] whereas at the same doses, Fe-NPs and $TiO_2$-NPs also exert toxicity to nontarget microbes and other biological entities. On the contrary, nanozerovalent iron exerted only adverse effects on soil microorganisms.[26] Hence, both the composition and functional competence of PGPR remain always under NP threat. The destructive impact of NPs on beneficial microbes could be due to one or simultaneous mechanisms, which include (i) alterations in cell surface morphology and growth behavior,[20] (ii) cell membrane disruption,[27] (iii) lipid peroxidation due to oxidative phosphorylation,[28] (iv) destruction of enzyme activity,[29] and (v) denaturation of proteins.[30] The toxicity of NPs to composition and functions of various organisms, however, differs with chemical composition, size, shape, surface charge, concentration, and period of exposure. Due to these, the assessment of NP−bacteria interactions vis-à-vis ecological balance becomes imperative.[31,32] In this context, very few attempts have been made to assess the biological, cytotoxic, and genotoxic impacts of NPs in controlled laboratory conditions and in soil on beneficial soil microflora. Furthermore, the knowledge on the adverse impacts of NPs on soil inhabitants is still limited. Considering the fact that NPs are discharged in the soil environment through various routes without proper treatment and their biological functions are completely different, it is reasonable to expect that the impact of NPs on the performance of soil bacteria and the bacteria−plant association will also differ while deposited in soils. To find ways as to how such threatening impacts of NPs can be curtailed, the present studies were designed to investigate (i) sensitivity of bacterial species toward various NPs, (ii) cellular respiration and membrane permeability, (iii) surface adsorption of NPs, cell topography, and morphology, (iv) fluorescence-based detection of cell death, (v) exopolysaccharide (EPS) production, (vi) bacterial growth under NP stress, (vii) superoxide and indole-3-acetic acid (IAA) production, and (viii) infrared (IR)-based detection of NP interaction with bacterial biomass.

## RESULTS

**Phenotypic Characterization of Bacterial Strains.** The strains of *Azotobacter chroococcum*, *Pseudomonas mosselii*, and *Sinorhizobium meliloti* were Gram-negative and rod-shaped, while *Bacillus thuringiensis* was found as Gram-positive with long rods (Figure S1). Each bacterial strain having varying morphological features (Table 1) produced different pigments when grown in their specific medium.

**Bacterial Population and NP Tolerance/Sensitivity.** The strains of *B. thuringiensis*, *P. mosselii*, *S. meliloti*, and *A. chroococcum* when grown in a culture-specific medium treated with various concentrations (62.5−1500 $\mu g\ mL^{-1}$) of Ag, ZnO, CuO, $Al_2O_3$, and $TiO_2$ showed differential resistance/sensitivity behavior. The minimum inhibitory concentration (MIC) and minimum bactericidal concentration (MBC) of Ag and ZnO-NPs against *B. thuringiensis*, *P. mosselii*, *S. meliloti*, and *A. chroococcum* are shown in Table 2. Among the NPs, CuO, $Al_2O_3$, and $TiO_2$ were found ineffective against bacterial strains even beyond the highest concentration (3000 $\mu g\ mL^{-1}$). The loss of bacterial cell viability was visible only at 62.5−1500 $\mu g\ mL^{-1}$ Ag-NPs and ZnO-NPs. The number of viable cells expressed as a colony-forming unit (CFU $mL^{-1}$) and as a function of Ag-NP and ZnO-NP concentration for *B. thuringiensis* (Figure S2), *P. mosselii* (Figure S3), *S. meliloti* (Figure S4), and *A. chroococcum* (Figure S5) was variable. The cell viability decreased consistently with increasing concentration of Ag-NPs and ZnO-NPs (Figure 1). The number of cells was found lowest at the corresponding MIC, which however was completely lost at MBC.

Table 2. MIC and MBC of Ag-NPs and ZnO-NPs against Beneficial Soil Bacteria

| | NPs ($\mu g\ mL^{-1}$) | | | |
|---|---|---|---|---|
| | Ag-NPs | | ZnO-NPs | |
| bacterial strains | MIC | MBC | MIC | MBC |
| *B. thuringiensis* | 1000 | 1500 | 1000 | 1500 |
| *P. mosselii* | 500 | 1000 | 500 | 1000 |
| *S. meliloti* | 250 | 500 | 500 | 1000 |
| *A. chroococcum* | 500 | 1000 | 250 | 500 |

**Measurement of Secondary Size and Ion Release Dynamics.** NPs of Ag and ZnO that were found to adversely affect the growth of test bacterial strains were analyzed for time-dependent (0−24 h) changes in secondary size and metal ion dissolution from NPs. The data revealed that size of both the NPs in nutrient broth solution increased in a time-dependent manner (Table S4). The secondary or hydrodynamic size of Ag-NPs increased from 244 ($t_0$ = 0 h) to 297 nm ($t_0$ = 24 h), while the size increase of ZnO-NPs was even more compared to Ag-NPs, i.e., 323 ($t_0$ = 0 h) to 352 nm ($t_0$ =


https://dx.doi.org/10.1021/acsomega.9b04084
ACS Omega 2020, 5, 7861−7876

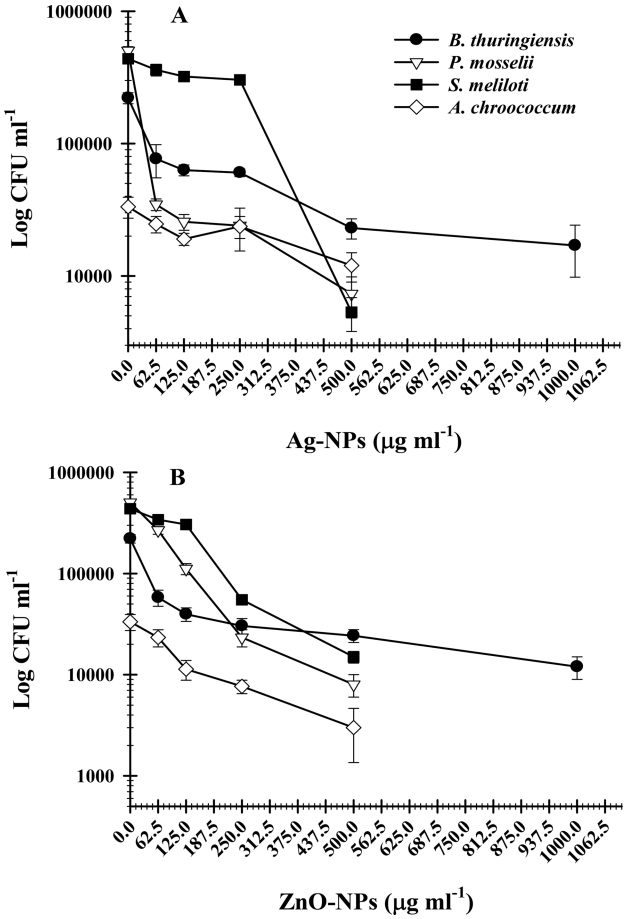


**Figure 1.** Concentration-dependent inhibition of bacterial cell viability by NPs. Curves show a decrease in the number of colony-forming units by (A) Ag-NPs and (B) ZnO-NPs.

24 h). However, ionic release from Ag-NPs was greater than ZnO-NPs at each time interval (Table S4).

**Measurement of Cellular Respiration under NP Stress.** The inhibition of cellular metabolism in terms of dehydrogenase activity was confirmed by the visible red color formation in untreated cells (Figure 2A). In contrast, the cell metabolic activity of all four bacterial strains was significantly reduced with increasing concentrations of Ag-NPs (Figure 2B) and ZnO-NPs (Figure 2C). In general, the reduction in absorbance ($\lambda_{max}$ = 450 nm) and hence loss of cellular respiration by both Ag-NPs and ZnO-NPs were found maximum at the highest test concentration of each NP.

**Production of IAA under Stress.** Among untreated bacteria, *P. mosselii* produced a maximum amount of 75.6 ± 3.8 $\mu$gIAA mL$^{-1}$ (Figure S6). After exposure of *P. mosselii*, *A. chroococcum*, and *S. meliloti* to 62.5−1000 $\mu$g mL$^{-1}$ each of Ag-NPs and ZnO-NPs, the IAA production by all bacterial strains decreased in a dose-dependent manner (Figure S6) when grown in a tryptophan (100 $\mu$g mL$^{-1}$) amended medium. Among NPs, Ag-NPs were found more toxic than ZnO-NPs for IAA secretion by *P. mosselii* and *A. chroococcum*, whereas ZnO-NPs exerted greater toxicity to *S. meliloti* and hence poor IAA secretion. While comparing the production of IAA at mean test concentration (387.5 $\mu$g mL$^{-1}$) of Ag-NPs by three bacterial strains, the *S. meliloti* showed maximum reduction (74%) in IAA secretion followed by *P. mosselii* (63%) and *A. chroococcum* (49%) over control (Table 3). Among all bacterial strains, ZnO-NPs (387.5 $\mu$g mL$^{-1}$) were found maximally inhibitory to *A. chroococcum* (72%). Overall, ZnO-NPs showed a maximum inhibitory effect (mean value, 20.3 $\mu$g mL$^{-1}$) on IAA production when compared to Ag-NPs (mean value, 24 $\mu$g mL$^{-1}$).

**Assessment of Bacterial Morphology under Ag-NP and ZnO-NP Stress.** The destructive potential of NPs against bacteria, when viewed under scanning electron microscopy (SEM), was variable (Figure 3). The surface of bacterial cells grown in the absence of NPs was smooth, while Ag-NPs and ZnO-NPs cells had a large number of gaps, pits, fragmented, and disorganized cell envelopes when grown in the presence of NPs. The surface of treated cells of *B. thuringiensis* appeared corrugated and had some depressions and alteration in length (Figure 3E−H). Broken and destructed cells were also observed for *P. mosselii* (Figure 3I−L). The compactness of treated cells increased significantly, which did not allow them to grow and divide further. Along with the irregular cellular architecture, single and multiple blisters were also noticed (Figure 3J,R). In treated *S. meliloti* cells, larger pits either on one or both cellular facets were noticed (Figure 3N,P). The MIC of Ag-NPs and ZnO-NPs induced the protrusion of numerous small bubbles in *A. chroococcum* cells (Figure 3R−T). Additionally, the exposure to NPs caused multiple dent formations and holes in all four bacterial cells envelopes.

**Atomic Force Microscopy of Bacterial Cultures under NP Stress.** The damage observed under SEM was supported by AFM data of control and treated cells of *P. mosselii* (Figure 4), *S. meliloti* (Figure 5), and *A. chroococcum* (Figure 6). Indeed, the 2D and 3D AFM images of untreated bacterial cells were homogeneous, while a strong heterogeneity was noticed after NP exposure. The NPs displayed distortion on the bacterial surface with varying degrees of surface roughness (panels E−H of Figures 4 to 6). The representative histogram for control, Ag-NP-, and ZnO-NP-treated cells are shown in Figure 4I−K (*P. mosselii*), Figure 5I−K (*S. meliloti*), and Figure 6I−K (*A. chroococcum*). The mean roughness was 12.6 ± 6 nm for untreated cells of *P. mosselii* and 58 ± 14 and 41 ± 7 nm for Ag-NP- and ZnO-NP-treated *P. mosselii*, respectively (Figure 4L). Similarly, the roughness for *S. meliloti* (Figure 5L) and *A. chroococcum* (Figure 6L) increased up to 38 ± 4 and 64 ± 11 nm under Ag-NP exposure, respectively, relative to control (24 and 20 nm). After ZnO-NP exposure, this increase was recorded to be 35 ± 4 and 45 ± 3 nm for *S. meliloti* and *A. chroococcum*, respectively.

**Surface Adsorption of NPs and Damage to the Cell Interior by HR-TEM.** The cell surfaces of control bacteria were clear of any particle-like structure (Figure S7A−D). On the other hand, when grown with Ag-NPs (Figure S7E−H) and ZnO-NPs (Figure S7I−L), the cells of *B. thuringiensis*, *P. mosselii*, *S. meliloti*, and *A. chroococcum* had NPs adsorbed onto their surfaces with small- or large-sized aggregates. Furthermore, the high-resolution transmission electron microscopy (HR-TEM) images of untreated cells showed a normal cell shape with an undamaged structure of the inner membrane and an intact slightly waved outer membrane. The internal cellular structure of untreated cells of *P. mosselii* (Figure 7A,B) and *A. chroococcum* (Figure 7E,F) appeared normal with a characteristic multilayered cell envelope consisting of an outer membrane, peptidoglycan layer, and a cytoplasmic membrane. Following the uptake of Ag-NPs and ZnO-NPs, cells of *P. mosselii* and *A. chroococcum* underwent massive transformation and had obvious damage (Figure 7C,D,G,H). The cells


https://dx.doi.org/10.1021/acsomega.9b04084
ACS Omega 2020, 5, 7861−7876

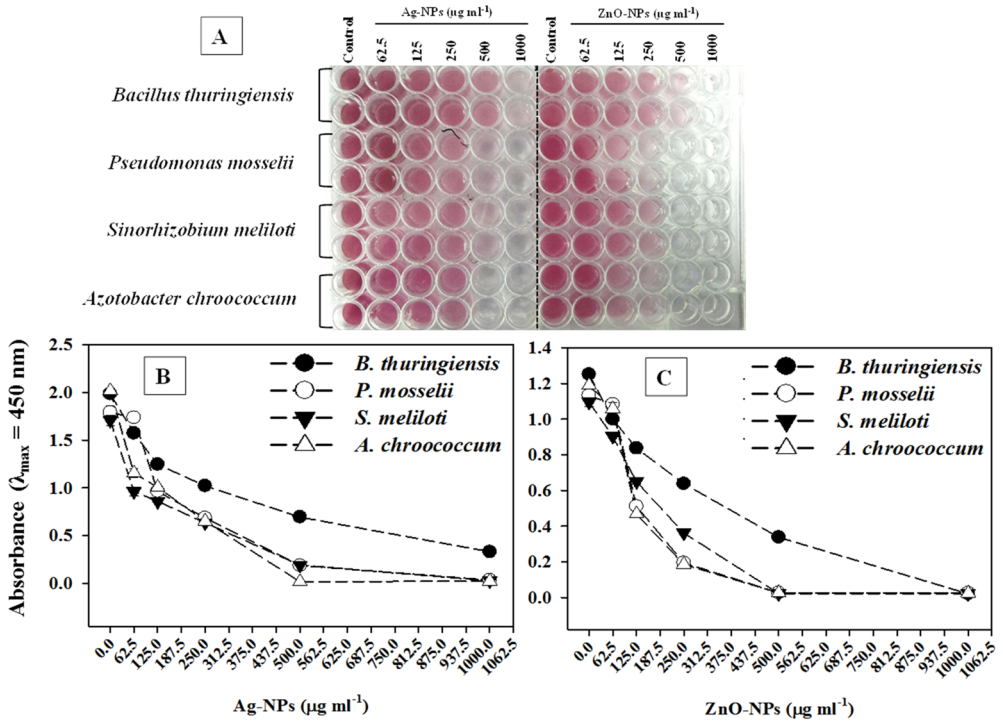


**Figure 2.** Inhibition of cellular respiration of *B. thuringiensis*, *P. mosselii*, *S. meliloti*, and *A. chroococcum* exposed to 62.5−1000 $\mu$g mL$^{-1}$ each of Ag-NPs and ZnO-NPs. (A) Decrease in red color intensity in microtiter wells represents the loss of metabolic activity of bacterial cells. (B, C) Spectrophotometric measurement of red colored formazan.

**Table 3. Production of IAA by Test Bacterial Strains**[a]

| | | IAA ($\mu$g mL$^{-1}$) | | | |
|---|---|---|---|---|---|
| treatment | mean concentration($\mu$g mL$^{-1}$) | *P. mosselii* | *S. meliloti* | *A. chroococcum* | mean value |
| control | 0 | 75.6 ± 3.87 | 46.2 ± 2.45 | 62.5 ± 4.63 | 61.4 |
| Ag-NPs | 387.5 | 27.7 ± 11.6 (63) | 12.1 ± 7.5 (74) | 32 ± 13.2 (49) | 24 |
| ZnO-NPs | 387.5 | 23.1 ± 13.8 (69) | 20.7 ± 10.14 (55) | 17.2 ± 10.6 (72) | 20.3 |

[a]Values are mean of three independent replicates; values in parenthesis indicate percent reduction in IAA secretion over control.

showed aberrant morphology, cracking, and disruption of the cell envelope. The leakage of the cytoplasmic content from the intracellular environment was apparent and can be clearly seen for *P. mosselii* and *A. chroococcum*. Electron-dense material was also noticed around damaged bacterial cells. Membrane-compromised cells showed localized separation of the cell membrane from the cell wall. The cellular degradation was also accompanied by empty cellular spaces in the cytoplasm.

**FTIR Analysis of NP-Treated Bacterial Biomass.** The Fourier transform infrared spectroscopy (FTIR) data of Ag-NP- and ZnO-NP-loaded dry biomass of *P. mosselii* (Figure 8A) and *A. chroococcum* (Figure 8B) revealed a significant deviation in the peaks corresponding to various functional groups of the bacterial cell surface. The IR signals in control and NP-treated *P. mosselii* and *A. chroococcum* are shown in Tables S1 and S2, respectively. Certain alterations were observed in the FTIR spectrum of the NP-treated bacterial cell biomass. Narrowing and shifting of peaks were observed. The electron micrographs, AFM images, and FTIR spectra of untreated and NP-treated biomass of *P. mosselii* and *A. chroococcum* thus clearly confirmed that Ag-NPs and ZnO-NPs had severe inhibitory effects on microbial cells and caused structural damage, leading to disturbances in the biochemical composition of the cells.

**Impact of NPs on Inner Membrane Permeability.** The plasma membrane allows bacterial cells to communicate with the surrounding environment and hence selectively facilitates the interfacial transport of molecules. To investigate the toxicity of NPs to the permeability of the membrane, the cells of *B. thuringiensis*, *P. mosselii*, *S. meliloti*, and *A. chroococcum* were exposed to a fixed concentration (1000 $\mu$g mL$^{-1}$) of Ag-NPs and ZnO-NPs (Figure 9). The enzyme $\beta$-galactosidase (an endoenzyme) is a frequently used stress marker to observe the injuries triggered by stressor molecules. The absorbance of *o*-nitrophenol (reaction product) in untreated cells of *B. thuringiensis*, *P. mosselii*, *S. meliloti*, and *A. chroococcum* was recorded to be 0.41, 0.32, 0.46, and 0.26, respectively. An increase in the absorbance of *o*-nitrophenol was noticed over control after Ag-NP exposure as 1.53, 1.87, 1.12, and 0.96 and after ZnO-NP exposure as 0.96, 1.24, 0.87, and 1.56 for *B. thuringiensis*, *P. mosselii*, *S. meliloti* and *A. chroococcum*, respectively. The enhanced release of $\beta$-galactosidase from the cell interior suggests an increase in cell membrane permeability.

**Confocal Laser Scanning Microscopy (CLSM) of Polysaccharide Matrix and Dead Cells.** Biofilms composing of cells and the glycocalyx matrix were stained by ConA-FITC and propidium iodide (PI). PI stains membrane-compromised cells red whereas ConA-FITC stains surround-


https://dx.doi.org/10.1021/acsomega.9b04084
ACS Omega 2020, 5, 7861−7876

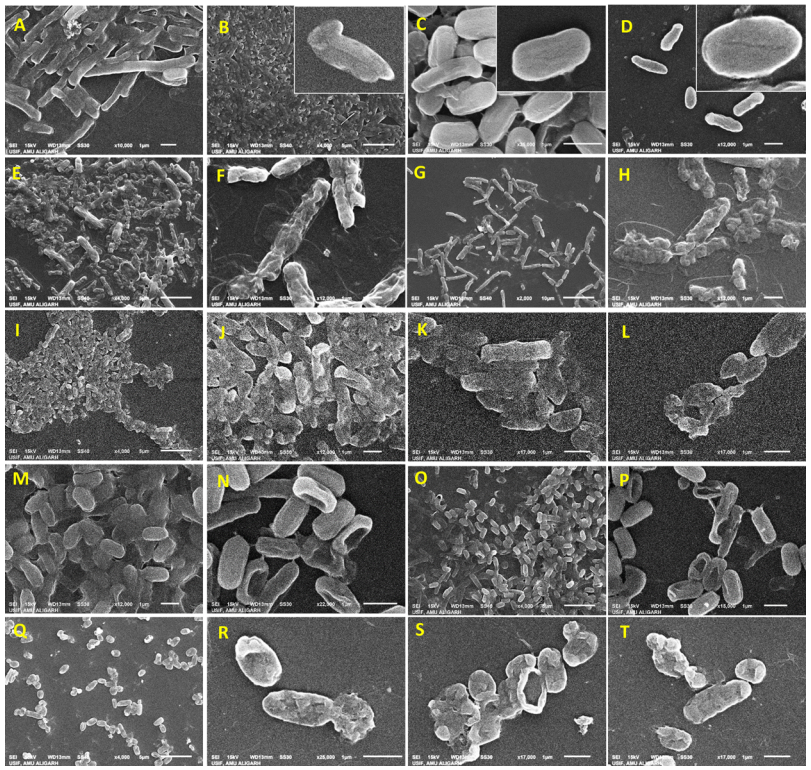

**Figure 3.** Scanning electron micrographs of (A) *B. thuringiensis*, (B) *P. mosselii*, (C) *S. meliloti*, and (D) *A. chroococcum* strain grown without NPs, *B. thuringiensis* strain grown with 1000 $\mu$g mL$^{-1}$ each of (E, F) Ag-NPs and (G, H) ZnO-NPs, *P. mosselii* strain grown with 500 $\mu$g mL$^{-1}$ each of (I, J) Ag-NPs and (K, L) ZnO-NPs, *S. meliloti* strain grown with 250 $\mu$g mL$^{-1}$ each of (M, N) Ag-NPs and (O, P) ZnO-NPs, and *A. chroococcum* strain grown with 500 $\mu$g mL$^{-1}$ each of (Q, R) Ag-NPs and (S, T) ZnO-NPs added to the NB culture medium.

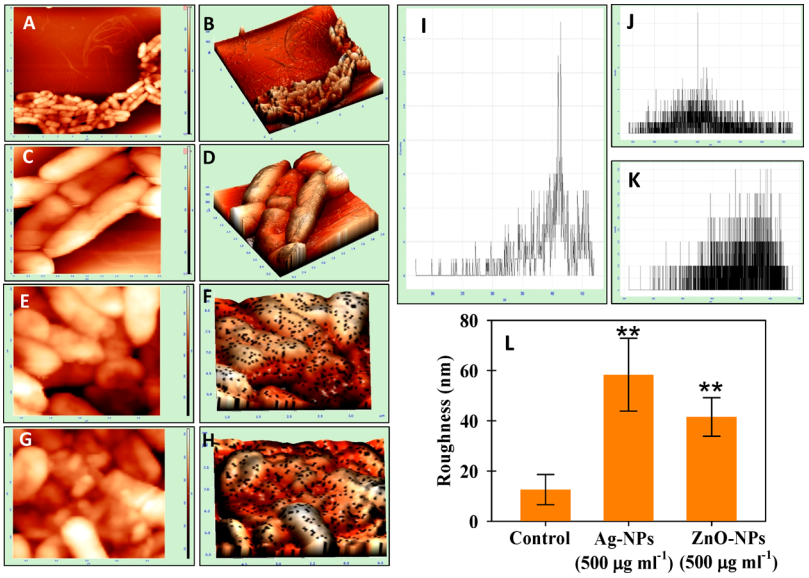


**Figure 4.** NPs induced morphological damage to the surface of *P. mosselii* measured by (A, C, E, G) two- and (B, D, F, H) three-dimensional AFM. (A–D) Control cells treated with (E, F) 500 $\mu$gAg-NPs mL$^{-1}$ and (G, H) 500 $\mu$gZnO-NPs mL$^{-1}$. (I–K) Representative histograms of the roughness of (I) control, (J) Ag-NP treatment, and (K) ZnO-NP treatment. (L) Statistical analysis of roughness (nm). The roughness was calculated from 10 cells for each treatment. Asterisks indicate significant difference at $P < 0.001$.

ing EPS green by binding to mannose residues. Inside the biofilm architecture, dark regions were attributed to water channels or the heterogeneity of the matrix. Overlay CLSM images yielded a yellow color, reflecting that EPS is produced as a capsular component in biofilm. Moreover, the bacteria cells were found encased in a scaffolding network of EPS, which suggests a 3D architecture of biofilms. The micrographs in panel (A) of Figures S8 to S11 exhibit the biofilm formation in the absence of NPs with a definite architecture. However, in the presence of Ag-NPs and ZnO-NPs, a scanty growth of *B. thuringiensis* (Figure S8B,C), *P. mosselii* (Figure S9B,C), *S. meliloti* (Figure S10B,C), and *A. chroococcum* (Figure S11B,C)


https://dx.doi.org/10.1021/acsomega.9b04084
ACS Omega 2020, 5, 7861−7876

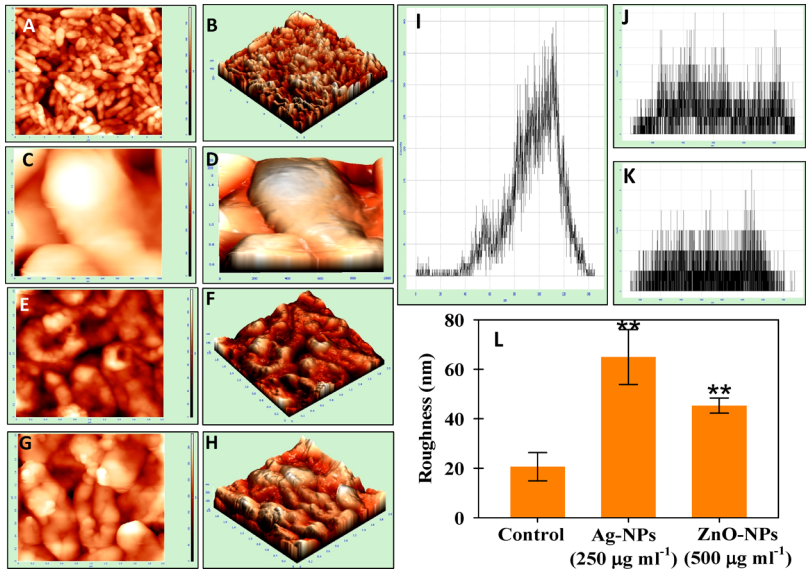


**Figure 5.** NPs induced morphological damage to the surface of *S. meliloti* measured by (A, C, E, G) two- and (B, D, F, H) three-dimensional AFM. (A–D) Control cells treated with (E, F) 500 $\mu$gAg-NPs mL$^{-1}$ and (G, H) 500 $\mu$gZnO-NPs mL$^{-1}$. (I–K) Representative histograms of the roughness of (I) control, (J) Ag-NP treatment, and (K) ZnO-NP treatment. (L) Statistical analysis of roughness (nm). The roughness was calculated from 10 cells for each treatment. Asterisks indicate significant difference at $P < 0.001$.

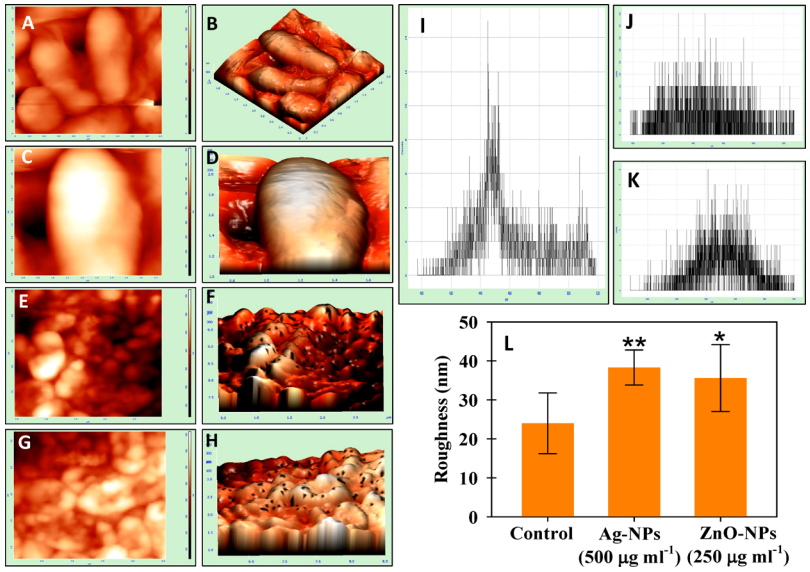


**Figure 6.** NPs induced morphological damage to the surface of *A. chroococcum* measured by (A, C, E, G) two- and (B, D, F, H) three-dimensional AFM. (A–D) Control cells treated with (E, F) 500 $\mu$gAg-NPs mL$^{-1}$ and (G, H) 500 $\mu$gZnO-NPs mL$^{-1}$. (I–K) Representative histograms of roughness of (I) control, (J) Ag-NP treatment, and (K) ZnO-NP treatment. (L) Statistical analysis of roughness (nm). The roughness was calculated from 10 cells for each treatment. Asterisks indicate significant difference at $*P < 0.05$ and $**P < 0.001$.

with lesser number of live cells and without a distinct pattern of cell arrangement was observed. The cells also exhibited morphological deformation upon exposure to NPs. Thus, the treatment of biofilms with NPs significantly restricted the colonization of bacterial cells, compared to the massive growth and biofilm formation by untreated cells. The NPs induced cell death and thus reduced EPS matrix around bacterial cells and a disrupted three-dimensional structure of the biofilm. Metabolically inactive cells appeared red against the black background when excited at 532 nm ($\lambda_{exc}$) due to binding of PI to bacterial DNA. In contrast, untreated cells exhibited none or residual red fluorescence.

***In Situ* Visualization of Surface Adherence under NP Stress.** To check the bacterial establishment, cells were grown *in vitro* with and without Ag-NPs and ZnO-NPs. The ability of test bacteria to adhere onto a solid surface such as polystyrene wells while growing with Ag-NPs and ZnO-NPs was measured using the crystal violet (CV) method and was found inhibited when compared to control (Figure 10). The control cells exhibited maximum retentions of CV to be 0.98, 1.15, 0.85, and 1.4 for *B. thuringiensis*, *P. mosselii*, *S. meliloti*, and *A. chroococcum*, respectively. The absorbance of CV for *B. thuringiensis* (Figure S12A), *P. mosselii* (Figure S12B), *S. meliloti* (Figure S12C), and *A. chroococcum* (Figure S12D)


https://dx.doi.org/10.1021/acsomega.9b04084
*ACS Omega* 2020, 5, 7861–7876

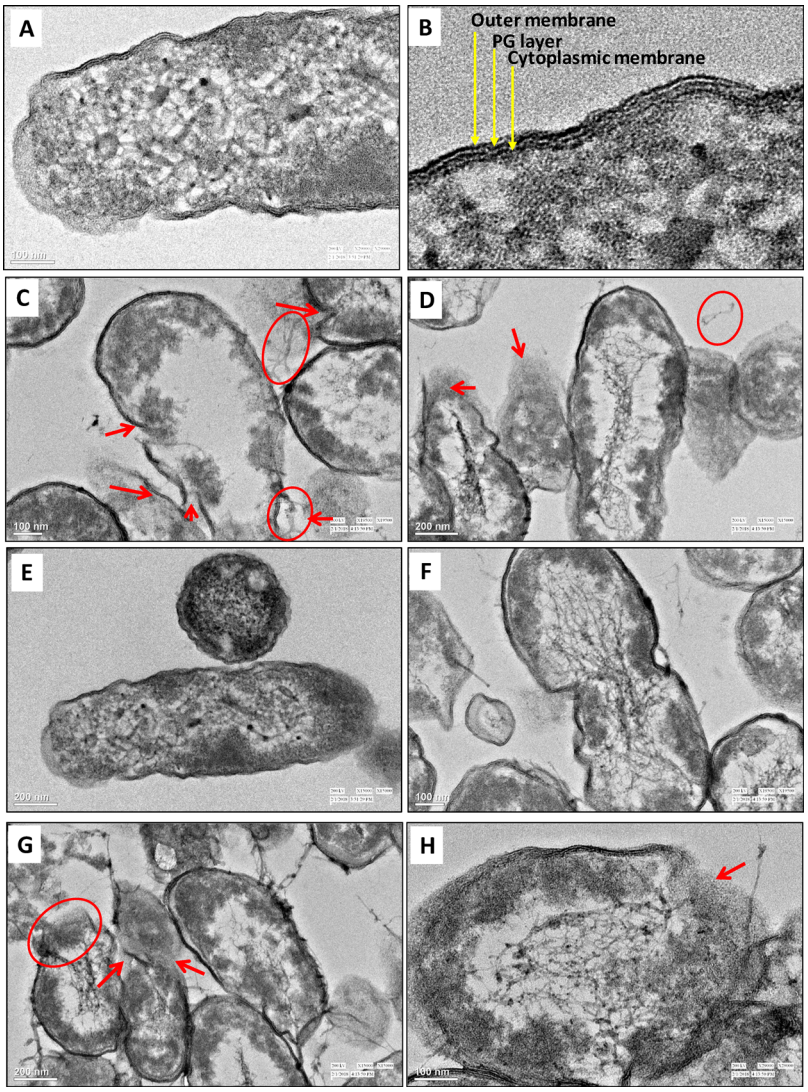


**Figure 7.** NP−bacteria interaction. HR-TEM images of untreated cells of (A) *P. mosselii*, (B) a magnified view of cell envelope, and after interaction with 500 $\mu$g mL$^{-1}$ each of (C) Ag-NPs and (D) ZnO-NPs, (E) untreated cells of *A. chroococcum*, (F) a magnified view of the cell envelope, and after interaction with 500 $\mu$g mL$^{-1}$ each of (G) Ag-NPs and (H) ZnO-NPs. Red circles show leakage of the cellular content, while arrows indicate cellular damage.

decreased under varying concentrations of Ag-NPs and ZnO-NPs.

**Bacterial Growth Curve under NP Stress.** The impact of NPs on the growth behavior of *B. thuringiensis* (Figure S13A,B), *P. mosselii* (Figure S13C,D), *S. meliloti* (Figure S13E,F), and *A. chroococcum* (Figure S13G,H) was variable. All sub-MIC concentrations of NPs delayed the growth of test bacterial strains. The growth curves of bacterial cultures had three phases: lag, exponential, and stationary. However, decline phases as seen under normal growth conditions were not observed. The growth of cells treated with the lowest concentration of NPs was also slightly lower than that of cells in the control group. When cells were exposed to a higher concentration of NPs, the growth of all bacterial strains was abolished.

**Generation of Superoxide Anions under NP Stress.** The $O_2^{\cdot-}$ radicals produced by *B. thuringiensis*, *P. mosselii*, *S. meliloti*, and *A. chroococcum* when grown in the presence of 62.5−1000 $\mu$g mL$^{-1}$ Ag-NPs and ZnO-NPs reduced the nitro blue tetrazolium (NBT) to formazan, which was assayed spectrophotometrically (Figure S14). The production of $O_2^{\cdot-}$ increased with an increasing concentration of NPs. Among NP concentrations, the Ag-NPs at 125−1000 $\mu$g mL$^{-1}$ and ZnO-NPs at 250−1000 $\mu$g mL$^{-1}$ were found more effective and induced maximally the production of $O_2^{\cdot-}$ by all bacterial strains. The data revealed a dose-related increase in $O_2^{\cdot-}$. While comparing the production of $O_2^{\cdot-}$ by all bacterial strains (Table 4), *B. thuringiensis* showed a maximum production of $O_2^{\cdot-}$ (0.78) when treated with a mean test concentration (387.5 $\mu$g mL$^{-1}$) of Ag-NPs, whereas *S. meliloti* at 387.5 $\mu$g mL$^{-1}$ ZnO-NPs showed the highest production (0.58) $O_2^{\cdot-}$.

## DISCUSSION

Among soil microorganisms, PGPR plays an important role in maintaining soil fertility and consequently crop health.[33] Due to these, understanding the potential impact of NPs on soil microflora that enhances the crop production by supplying essential biomolecules becomes important to assess the overall impact of NPs on agricultural ecosystems. To date, there are limited studies available on the interaction between NPs and


https://dx.doi.org/10.1021/acsomega.9b04084
ACS Omega 2020, 5, 7861−7876

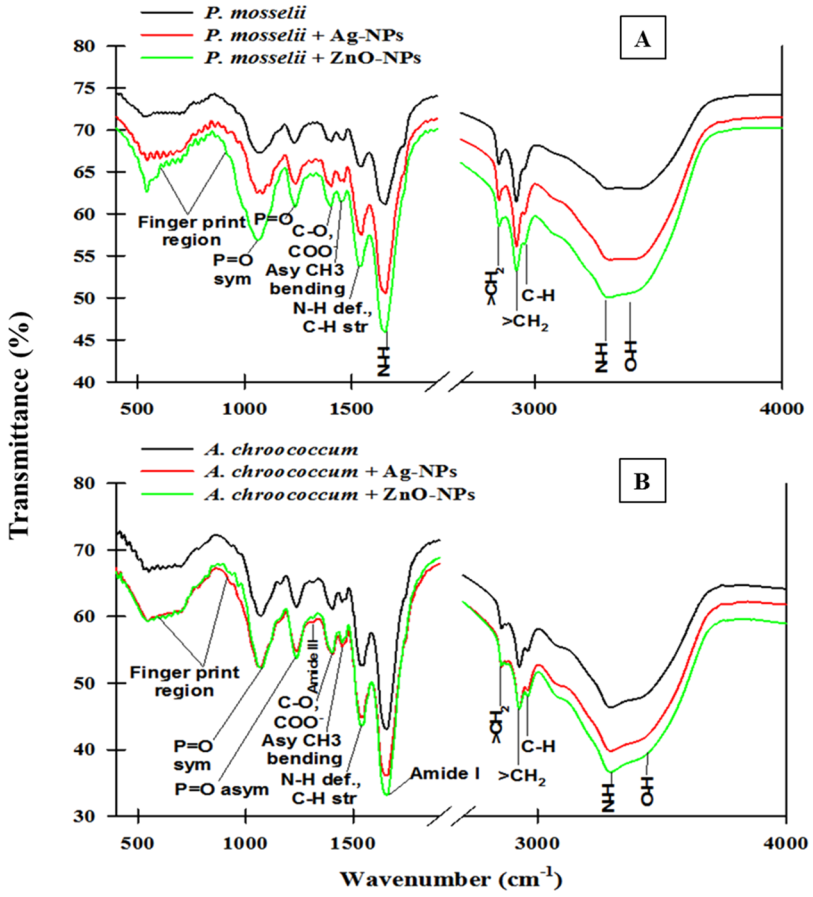


**Figure 8.** FTIR Spectra of the biomass of (A) *P. mosselii* after 24 h and (B) *A. chroococcum* after 3 days of growth in nutrient broth amended with 500 $\mu$g mL$^{-1}$ each of Ag-NPs and ZnO-NPs.

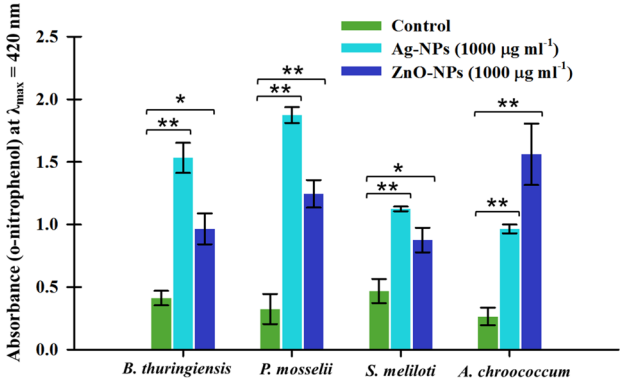


**Figure 9.** Extracellular $\beta$-glycosidase activity of *B. thuringiensis*, *P. mosselii*, *S. meliloti*, and *A. chroococcum* exposed to 1000 $\mu$g mL$^{-1}$ each of Ag-NPs and ZnO-NPs. Absorbance of *o*-nitrophenol at 420 nm is plotted against NP concentrations. Values are mean of three independent replicates ± SD. Asterisks indicate significant difference at *$P$ < 0.05 and **$P$ < 0.001.

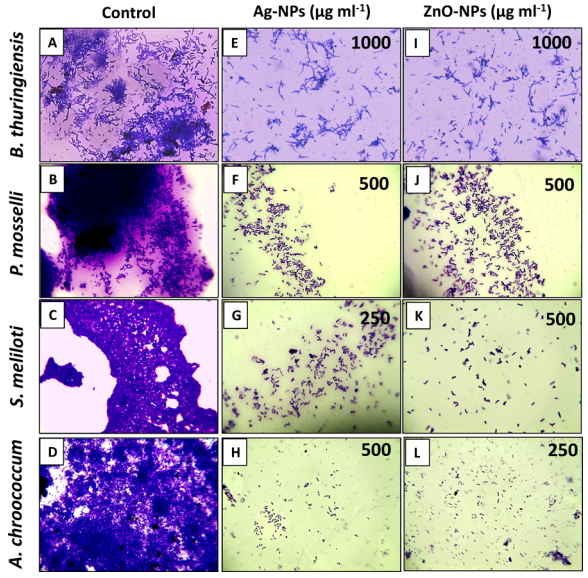


**Figure 10.** Inhibition of bacterial colonization on the surface of polystyrene wells. (A–D) Micrographs of untreated bacterial cells, (E–H) cells treated with MIC of Ag-NPs, and (I–L) cells treated with MIC of ZnO-NPs.

beneficial bacteria and related species. Hence, the present study was undertaken to assess the impact of five NPs (ZnO, CuO, $Al_2O_3$, $TiO_2$, and Ag) on growth, morphology, and physiological activity of *A. chroococcum*, *B. thuringiensis*, *P. mosselii*, and *S. meliloti*.

Arrest of bacterial growth was exhibited only by ZnO-NPs and Ag-NPs (Figures S2 to S5), whereas the CuO-NPs, $Al_2O_3$-NPs, and $TiO_2$-NPs tested at even higher doses (1500–3000 $\mu$g mL$^{-1}$) were tolerated by bacterial species. The toxicity of NPs toward bacterial cells depends on bacterial species, metal oxide species,[34] and concentration of NPs.[35] This tolerance behavior could be due to the fact that bacterial cells have evolve some defense mechanisms to protect themselves from


https://dx.doi.org/10.1021/acsomega.9b04084
ACS Omega 2020, 5, 7861–7876

Table 4. Production of Superoxide Anions by Test Bacterial Strains

| | | mean absorbance (λ520 nm) | | | |
|---|---|---|---|---|---|
| treatment | mean concentration($\mu$g mL$^{-1}$) | *B. thuringiensis* | *P. mosselii* | *S. meliloti* | *A. chroococcum* |
| control | 0 | 0.21 | 0.12 | 0.23 | 0.18 |
| Ag-NPs | 387.5 | 0.78 | 0.67 | 0.54 | 0.46 |
| ZnO-NPs | 387.5 | 0.52 | 0.51 | 0.58 | 0.46 |

harmful stressors, including NPs.[36] In agreement with the present findings, $TiO_2$-NPs have shown a negligible shift in the bacterial community composition.[37] The variation in tolerant behavior of bacterial species could be due to (i) structural changes in the cell envelope: the peptidoglycan (PG) and phospholipid component of either Gram-negative or Gram-positive bacterial cells is the first line of defense,[38] which responds to a stress stimulus by one of the following mechanisms: (a) production of alternative extra-cytoplasmic function sigma ($\sigma$) factors regulating the expression of genes with unknown or known functions[39] like the biogenesis of lipopolysaccharides (LPS). These $\sigma$-factors influence the incorporation of D-alanine into the polyanionic techoic acids (TAs), which are negatively charged. This in turn reduces the net negative charge on the cell wall of Gram-positive bacteria, thereby reducing the electrostatic attraction of positively charged metal oxide NPs and (b) activation of two component signal transduction system such as the conjugative pilus expression (Cpx) system, which regulates the expression of a wide variety of genes and proteins, for example, the expression of virulence factors like pili/fimbriae factors.

(ii) Physiological changes: both Gram-negative and Gram-positive bacteria can accumulate electron-dense granules/particles at the center of the cell. This is nothing but the thicker DNA molecules, and this thickness enables the protection against metal ions.[40,41] (iii) Efflux pumps: efflux pumps embedded in the bacterial cell membrane can efficiently pump out the toxic metal ions,[36] which are released from NPs.[42] The encoding of this efflux pump is carried out by the plasmid-borne cassettes. (iv) Molecular changes: this includes adaptive/point mutations and plasmids with resistance encoding genes.[43] Apart from the neutral behavior of CuO, $Al_2O_3$, and $TiO_2$-NPs in the current study, the $TiO_2$-NPs in an earlier study showed enhanced survival of *Bacillus subtilis* by disrupting its autolysis.[44] Molecular analysis revealed two possible routes of $TiO_2$-NP-mediated autolysis prevention either directly via attachment of $TiO_2$-NP on the cell wall, delaying the collapse of the PMF, and thus autolysis or via adsorption of *B. subtilis* autolysins on $TiO_2$-NP, thereby reducing autolysin activity.[44]

The reduction in bacterial cell viability (Figures S2 to S5) could be due to many reasons: chief among them is the loss of bacterial cell respiration that was assayed using the 2,3,5-triphenyltetrazolium chloride (TTC)-based spectroscopic method (Figure 2). TTC in the presence of an electron donor such as NADH and cellular dehydrogenase (e.g., succinate dehydrogenase) forms a red color product triphenyl formazan (TPF), which is an indicator of cellular metabolism.[28] In agreement with the present study, inhibition of bacterial cell respiration using the TTC assay has been reported for four clinical bacterial isolates.[45] Moreover, respiratory inhibition by Ag-NPs in nitrifying bacteria has also been reported,[46] which has been due to the interaction of NPs with components of the bacterial plasma membrane, leading to respiratory inhibition. Furthermore, it has been observed that the NPs cause cellular disintegration and produce oxidative damage.[20] The higher toxicity of Ag-NPs was correlated with a smaller size. In similar experiments, Gambino et al. and Zhang et al. explored the toxicity of NPs on soil bacteria *B. subtilis* and *Azotobacter vinelandii*, respectively.[20,47] The phytohormone auxin (IAA) is synthesized by many plant beneficial rhizobacteria,[48,49] which regulates the developmental and physiological processes of plants, including cell division, cell enlargement, phototropism, initiation of root growth, and apical dominance.[50] In this study, Ag-NPs and ZnO-NPs decreased IAA synthesis by *P. mosselii*, *S. meliloti*, and *A. chroococcum* consistently to the extent that it became almost negligible at the highest concentration (1000 $\mu$g mL$^{-1}$) of each NP (Figure S6). The Ag-NPs were found more toxic than ZnO-NPs for IAA secretion by *P. mosselii* and *A. chroococcum*, whereas ZnO-NPs exerted greater toxicity to IAA secretion by *S. meliloti*. In an experiment, the decline in IAA secretion by symbiotic $N_2$ fixing *Bradyrhizobium japonicum* when exposed to varying rates of metals (5−500 $\mu$g mL$^{-1}$) has been reported.[51] The reduction in IAA production at higher NP concentrations could possibly be due to slower growth and altered physiological activity of bacterial cells. In line with these results, the growth inhibition and expression profile of selected genes in model nitrogen-metabolizing bacteria exposed to quantum dots (QDs)[52] and Ag-NPs[53] has been reported.

Although the destructive effects of NPs on the structure, composition, and physiological activities of bacteria are well documented, the extent of damage to soil bacteria caused by NPs is rarely explained. Using two sensitive and target-specific microscopic techniques such as SEM[54] and AFM,[55] the variation in morphology of bacterial cells exposed to 1000 $\mu$g mL$^{-1}$ Ag-NPs and ZnO-NPs was determined. The NP-treated bacterial cells had a large number of gaps, pits on both cellular facets, fragmented, and disorganized cell envelope over untreated control cells (Figure 3). Similar morphological disruptions in *A. vinelandii* cells have been seen under SEM when cells were exposed to 100 $\mu$g mL$^{-1}$ Ag-NPs.[20] The morphological destruction caused to two beneficial bacteria *Bacillus amyloliquefaciens* and *Pseudomonas fluorescens* while grown with ZnO-NPs has been reported.[56] The destruction of cells by NPs could be attributed to an accumulation of such toxic NPs in the bacterial membrane, which might have altered the membrane potential, eventually leading to cell death. Beside the uptake of NPs, the release of $Ag^+$ and $Zn^{2+}$ ions form Ag-NPs and ZnO-NPs in a time-dependent manner; however, a little but may also contribute to the toxic impact of NPs (Table S4). The increased roughness suggested disorganization of the cell wall and correlates with the cell debris due to cellular destruction observed under SEM. Together, these results revealed morphological, mechanical, and physical damage to the bacterial cell wall. The treated cells (Figures 4 to 6) displayed distortion on the surface with varying degrees of roughness. The mean value of cell roughness (nm) was higher and statistically significant ($P <$


https://dx.doi.org/10.1021/acsomega.9b04084
ACS Omega 2020, 5, 7861−7876

0.05) after exposure to NPs over control. Ag-NPs caused a higher degree of roughness compared to ZnO-NPs. This increase in roughness and amorphous mass could be associated with the perforation of the cell wall with the release of the intracellular material and subsequent cell wall deformation.[57] Similar topological change in *B. subtilis* cells exposed to a conjugate of siRNA/Ag-NPs−Qe at 20 $\mu$M has been revealed under AFM.[58]

HR-TEM analysis of bacterial cells grown in a liquid medium with NPs revealed considerable adsorption of NP aggregates on the cell surface (Figure S7) with a cracked and disrupted cell envelope. The NPs in effect caused an obvious disruptive impact on cellular morphology of test bacterial strains. Similar to our study, TEM micrographs of Ag-NP-treated *A. vinelandii* indicated rough and fuzzy membrane edges with leakage of substances inside the cells.[20] This could be due to the adsorption of Ag-NPs on to the cell membrane surface, which might have disrupted the membrane and wall. A fraction of NPs may even reach the cytoplasm and interact with the other cellular components, causing leakage of cytoplasmic contents.[20] In this study, membrane-compromised cells showed localized separation of the cell membrane from the cell wall accompanied by empty cellular spaces in the cytoplasm. It is clear from the results that NPs of Ag and ZnO anchored the bacterial cell at several locations and caused subsequent damage to the cell envelope, which ultimately resulted in cell lysis. More so, the resulting damaged structure was an empty intact cell envelope devoid of the cytoplasmic content, sometimes called "ghost cells".[59] Indeed, the distortion of the physical structure of the cell could cause the expansion and destabilization of the membrane. It increases membrane fluidity and thus passive permeability and leakage of various vital intracellular constituents. Similarly, disruption with consequent release of intracellular materials from *Staphylococcus aureus* cells leaving behind empty and flaccid cells has been reported.[57] Furthermore, the change in functional groups of bacterial surface proteins and lipids was detected by the FTIR technique (Figure 8). The shift in peaks (compared to control) could possibly be due to the changes in functional groups present on the bacterial cell surface as a result of interaction with various NPs. Studies have shown that the reaction of sulfur-containing membrane proteins with NPs may lead to inactivation of membrane-bound enzymes and proteins,[29,60] which in turn increases the passive permeability and facilitates the leakage of vital intracellular constituents.[57]

The change in cell membrane permeability was confirmed by PI staining of (Figures S8 to S11). In a dual staining method, the concanavalin-A component of ConA-FITC, which has binding affinity binds to mannose residues of surrounding EPS,[61] indicated bacterial biofilm formation under CLSM analysis. The extracellular release of $\beta$-galactosidase indicated damage to inner membrane permeability of bacterial cells (Figure 9). Conventionally, the untreated control cells did not show any red fluorescence. Mechanistically, the PI dye (a DNA intercalating dye) permeates only through the membranes of dead cells, and hence, the cells become red in color.[62] EPS are polymeric substances synthesized by soil microbes as a protective material to overcome many stressful conditions[63] and also essential for successful adhesion of bacterial cells to plant roots and thus improve plant performance. The toxicity of Ag-NPs and ZnO-NPs was confirmed by inhibition of EPS production by cells of *B. thuringiensis*, *P. moselli*, *S. meliloti*, and *A. chroococcum* and thus their ability to attach to a solid surface (Figure 10 and Figure S12). EPS production favors the adsorption of NPs on the bacterial surface and subsequently resulted in enhanced membrane disruption. The results obtained with the double-staining technique revealed that NPs induced cell death and inhibited EPS matrix around bacterial cells, resulting in a disrupted three-dimensional structure of biofilm. This inhibitory effect of NPs on the biofilm could be attributed to the malfunctioning of water channels throughout the biofilm, which are present for nutrient transportation. Additionally, NPs may directly diffuse through the EPS layer and impart antimicrobial action, and due to this, metabolically inactive cells appeared red against the black background. In agreement with our findings, a decrease in EPS production by bacterial cells exposed to Ag-NPs has been reported.[64] A correlation between toxicological data and physicochemical parameters of MONPs revealed that the toxicity increases as the hydration enthalpy becomes less negative and as the conduction band energy approaches those of biomolecules.[34]

In the current study, time (0−16 h)- and concentration (125−1000 $\mu$g mL$^{-1}$)-dependent growth behavior of test bacterial strains toward Ag-NPs and ZnO-NPs revealed differential growth patterns (Figure S13). All concentrations of NPs showed poor bacterial growth, in general, over untreated cells that were found almost negligible at the highest concentration. In a similar study, the growth of *A. vinelandii* was inhibited markedly when exposed to 2−100 mg l$^{-1}$ Ag-NPs for 48 h.[20] Moreover, the generation of reactive oxygen species such as superoxide anions ($O_2^{\cdot-}$) by NPs has been considered as one of the primary factors causing significant bacterial killing.[22] In our study, the production of superoxide anions detected by the NBT assay increased with increasing concentration (62.5−1000 $\mu$g mL$^{-1}$) of Ag-NPs and ZnO-NPs (Figure S14). The variation in the production of $O_2^{\cdot-}$ under NP stress could be due to the difference in architecture and composition of bacterial cells. In a related study, exposure of two bacterial strains to ZnO-NPs has shown an increase of 26−83% in SOD activity, which could be due to the formation of $O_2^{\cdot-}$.[65] Although all mechanisms of NP interaction with bacterial cells are not well known, NPs can affect multiple target sites of the microbial cells simultaneously such as the cell membrane,[66] enzymes/proteins,[22] lipids,[67] DNA, and plasmids.[68] The antibacterial activity of NPs might also be due to the release of metal ions ($Zn^{2+}$ and $Ag^{+}$) from the NPs (e.g., ZnO and Ag).[69] However, in our case, the release of ions from NPs was too low to exert any significant negative impact (Table S4). Broadly, the bacterial cell suppression/inhibition due to the Ag-NP or ZnO-NP action may involve the following steps: (i) adsorption of NPs on the bacterial surface (wall and membranes) via electrostatic attraction due to the surface potential, (ii) distortion of cell morphology/topography, (iii) uptake of NPs and their release into the periplasm and cytoplasm along with ions due to bacterium-assisted transformation of NPs, (iv) membrane damage due to increased porosity, structural, and functional interruption, (v) leakage of cytoplasmic and nuclear materials, (vi) destruction of cellular respiration, (vii) inhibition of ability to synthesize bioactive molecules like IAA, (viii) generation of intracellular oxidative stress (superoxide anions), which further magnifies the damage to cellular constituents and membranes, (ix) destruction of EPS secreting ability, and (x) eradication of surface adhering potential of bacteria. These mechanisms may act independently or simultaneously. Based on these and according to the


https://dx.doi.org/10.1021/acsomega.9b04084
ACS Omega 2020, 5, 7861−7876

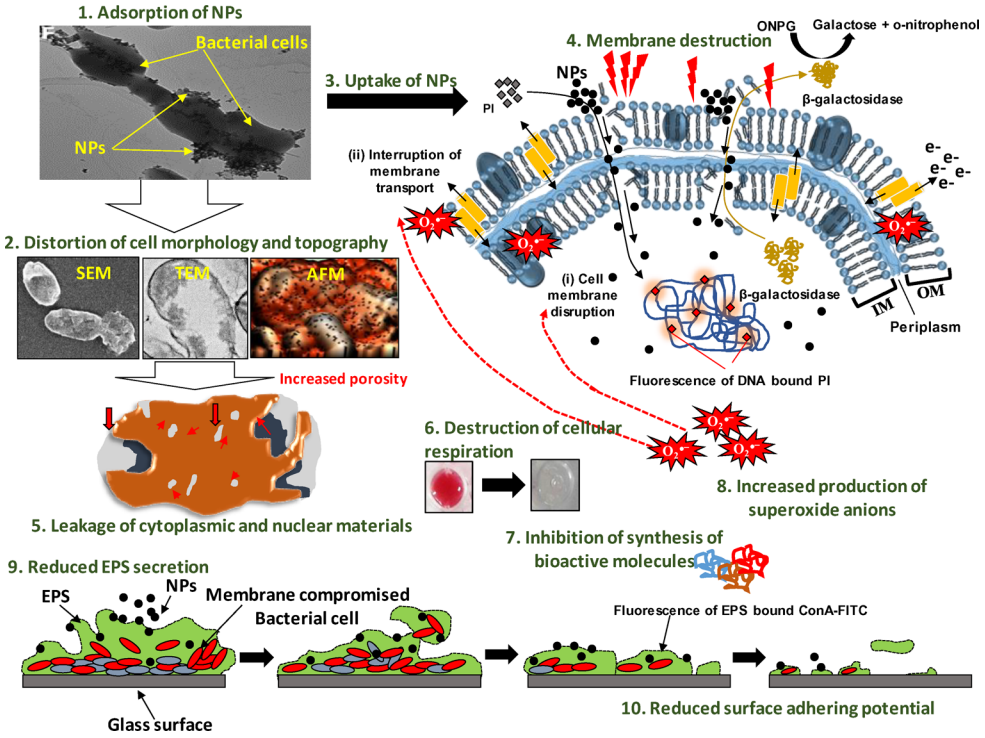


**Figure 11.** Proposed mechanism of Ag-NP and ZnO-NP toxicity to soil bacteria.

results obtained in our study, stepwise and systematic events of NP action on bacterial cells can be summarized as displayed in Figure 11.

## CONCLUSIONS

Four metal oxide NPs (ZnO, CuO, $Al_2O_3$, and $TiO_2$) and one metal NP (Ag) were tested against four beneficial bacterial isolates *B. thuringiensis*, *A. chroococcum*, *P. mosselii*, and *S. meliloti*. Among them, Ag-NPs and ZnO-NPs caused extensive damage to all strains; however, bacterial cells showed tolerance toward the NPs of CuO, $Al_2O_3$, and $TiO_2$ up to 3000 $\mu g\ mL^{-1}$. This could be due to the fact that the toxicity of NPs against bacterial cells depends on bacterial species and composition of NPs. Bacterial cells have also evolved some defense mechanisms to protect themselves from harmful stressors, including NPs. Bacterial respiration and the number of CFU $mL^{-1}$ decreased consistently with an increasing dose rate of Ag-NPs and ZnO-NPs. Attachment of NPs prepared from Ag and ZnO on bacterial cells facilitated their uptake inside the cells, which eventually resulted in cell roughness, morphological destruction, and leakage of the cytoplasmic content coupled with a loss of the IAA producing ability, increased cell membrane permeability, and reduced EPS production. Ag-NPs and ZnO-NPs enhanced superoxide generation, reducing the surface adhering potential of cells and growth kinetics. Conclusively, a plausible mechanism of NP toxicity to beneficial bacteria has been explored. Due to high demands of nanoenabled products in various industries and their unregulated discharge in the environment may affect the useful bacterial population, a holistic approach for the disposal and recycling of nanowaste must be adopted.

## EXPERIMENTAL SECTION

**NPs of Ag, CuO, $Al_2O_3$, $TiO_2$, and ZnO.** The NPs of CuO, $Al_2O_3$, $TiO_2$, and ZnO used in the current study were the same, as described by Ahmed et al.,[70] whereas Ag-NPs were synthesized by a green chemistry method using quercetin dihydrate, as discussed elsewhere.[71] All NPs were well characterized physicochemically, and size, shape, morphology, topography, chemical composition, aqueous behavior, and spectroscopic signals of each NP were determined.[70,71] The summary of physicochemical characteristics of NPs is given in Table S3. Impact of the nutrient medium on 1000 $\mu g\ mL^{-1}$ concentration of NPs while kept on shaking (150 r/min for 24 h) on the secondary size (measured by DLS) and metal ion release (measured by ICP-MS) from Ag-NPs and ZnO-NPs is given in Table S4.

**Maintenance of Bacterial Cultures.** The bacterial strains possessing plant growth-promoting properties such as *A. chroococcum* Beijerinck 1901 (ATCC 9043), *B. thuringiensis* (2095), and *P. mosselii* (2126) were procured from the National Centre for Microbial Resource (NCMR; Pune, India), whereas nodule bacterium *S. meliloti* (NAIMCC-B-00863) was obtained from the culture collection of the National Bureau of Agriculturally Important Microorganisms (NBAIM; Mau, India) (Table S5). Strains of *A. chroococcum*, *B. thuringiensis*, *P. mosselii*, and *S. meliloti* were maintained on Ashby's mannitol agar, nutrient agar, King's B medium, and yeast extract mannitol agar, respectively.

**Sensitivity of Bacterial Strains toward NPs.** The bacterial strains were checked for their sensitivity/resistance against various concentrations of Ag, ZnO, CuO, $Al_2O_3$, and $TiO_2$-NPs. An individual colony of each strain was inoculated in 100 mL of capacity flasks containing 50 mL of culture-specific broth amended with 62.5, 125, 250, 500, 1000, and 1500 $\mu g\ mL^{-1}$ of each NPs. The untreated (control) and treated cultures of *B. thuringiensis*, *P. mosselii*, and *S. meliloti* were incubated at 28 °C for 24 h in a shaking incubator (100 r/min), whereas *A. chroococcum* was incubated for 72 h while other growth conditions remained identical. A 0.1 mL bacterial


https://dx.doi.org/10.1021/acsomega.9b04084
ACS Omega 2020, 5, 7861−7876

culture was uniformly spread on a semisolid agar medium and allowed to incubate as mentioned above. MIC and MBC were determined. The MIC was defined as the lowest dose of NPs that prevented bacterial growth maximally (99%), whereas the minimum dose of NPs that killed all cells in the broth was considered as MBC. The cell viability was counted as CFU $mL^{-1}$ employing the formula

$$\text{CFU mL}^{-1} = \frac{\text{number of colonies} \times \text{dilution factor}}{\text{volume plated (mL)}}$$

The number of CFU $mL^{-1}$ was converted to a logarithmic scale (log CFU $mL^{-1}$) and plotted as a function of NP concentration ($\mu$g $mL^{-1}$).

**Impact of NPs on Inner Membrane Permeability.** The $\beta$-galactosidase (an endoenzyme) activity of bacterial cultures was assayed using *o*-nitrophenyl-$\beta$-D-galactopyranoside (ONPG; HiMedia, India) as a substrate to check the permeability of the inner membrane. For this, bacterial cultures, namely, *A. chroococcum*, *B. thuringiensis*, *P. mosselii*, and *S. meliloti*, were grown in their respective medium supplemented with 2% lactose. Bacterial cells grown to an exponential level were separated by centrifugation and resuspended in 0.02 M sodium phosphate buffer (pH 7.5) containing NaCl (0.1 M). The cell density was maintained at $10^{8\text{-}9}$ CFU $mL^{-1}$. A 500 $\mu$L cell suspension from each treatment was mixed with 1000 $\mu$g $mL^{-1}$ Ag-NPs and ZnO-NPs separately and appropriately diluted from the ultrasonicated NP stock. The mixture was incubated at 28 °C with shaking for 4 h at 100 r/min followed by centrifugation. The supernatant was used to measure galactose and *o*-nitrophenol spectrophotometrically at 420 nm.

**Measurement of Cellular Respiration under NP Stress.** Inhibition of bacterial cellular respiration was determined by the dehydrogenase assay method.[72] In brief, cells of *A. chroococcum*, *B. thuringiensis*, *P. mosselii*, and *S. meliloti* grown to the early exponential growth phase were harvested at 5000 r/min for 10 min. Cells were resuspended in 1× sterile phosphate buffer saline (PBS; pH 7.0) to achieve an absorbance ($\lambda$ = 600 nm) of 0.4, and 200 $\mu$L of this cell suspensions was then transferred to wells in a 96-well microtiter plate. To each well, Ag-NPs and ZnO-NPs (62.5−1000 $\mu$g $mL^{-1}$) were added. Cell suspensions without NPs served as control. Subsequently, 40 $\mu$L of the reagent TTC (0.5%, w/v) was added to each well and allowed to incubate at room temperature (RT) for 30 min. After a 30 min incubation, the conversion of colorless solution to red was measured at 450 nm using a microplate reader (Thermo Scientific Multiskan EX, ref 51118170, China).

**Morphology and Topography of Bacterial Cells Influenced by NPs.** The changes in bacterial morphology following exposure to NPs was viewed under SEM. Cells of *A. chroococcum*, *B. thuringiensis*, *P. mosselii*, and *S. meliloti* were grown in 100 mL of capacity flasks containing a strain-specific nutrient broth to a level of $10^{7\text{-}8}$ CFU $mL^{-1}$. Then, 1000 $\mu$g $mL^{-1}$ each of Ag-NPs and ZnO-NPs were added to bacterial cells and further incubated on a rotatory shaker (100 r/min) for 12 h at 28 °C. After incubation, untreated control cells and cells treated with NPs were centrifuged (at 5000 r/min) for 10 min. The pellets were washed thrice with sterile PBS (1×) and fixed with 2.5% glutaraldehyde and 2% paraformaldehyde for 4 h at 4 °C with intermittent vortexing. The cells were successively washed three times with 1× PBS and dehydrated by ethanol gradient (30, 50, 70, 90, and 100%) for 10 min each. The cell biomass was then fixed on a 18 × 18 mm glass coverslip by air drying and sputter-coated with a 2 nm thin layer of gold. The coated samples were visualized under JSM 6510LV SEM at an accelerating voltage of 10 kV. AFM was used to reveal topographical images of the bacterial cell surface. For AFM analysis, bacterial cells grown at the exponential phase were immobilized on a glass cover slip by drying in sterile air and observed under an atomic force microscope (NT-MDT-NTEGRA, Moscow, Russia) and images were processed using the software NT-MDT solver Nova 1.0.26.1424. Morphological damage was evaluated by statistical analysis of surface roughness (nm) from AFM images. Roughness (nm) of bacterial cells was measured after fitting the lines in 1D and subtracting the second- and third-order surfaces. Data from 10 bacterial cells for each concentration were averaged and statistically presented as mean ± SD.

**Surface Adsorption and Cellular Destruction.** The attachment of NPs on the cell surface and cellular damage was detected by employing HR-TEM. Bacterial cultures were grown and treated as described for SEM analysis. After dehydration in ethanol series, specimens were embedded in white resin overnight. Ultrathin sections of specimens measuring nearly 50−70 nm were prepared by ultramicrotomy using a microtome diamond knife. Sections were stained with uranyl acetate (2%; Sigma-Aldrich, USA) followed by counter staining with lead citrate (2%; Sigma-Aldrich, USA). The sections were mounted on carbon-coated Cu grids and examined under Technai HR-TEM (FEI, Electron Optics, USA) at 120 kV.

**FTIR Analysis of NP-Treated Bacterial Biomass.** The biomolecular alterations in cell surface functional groups induced by 500 $\mu$g $mL^{-1}$ each of Ag-NPs and ZnO-NPs in *P. mosselii* and *A. chroococcum* were analyzed by FTIR. The bacterial cultures used as model strains were first grown for 48 h at 28 °C and then treated with 500 $\mu$g $mL^{-1}$ concentration of each NP. After a 24 h incubation, the biomass prepared from both NP-treated and untreated bacterial strains were analyzed by an FTIR spectrometer. For this, 2.5 mg of biomass dried at 60 °C under vacuum was ground with 75 mg of KBr in an agate mortar. The translucent discs were prepared by putting tons of pressure on the material using a bench press. The prepared discs were scanned in the range of 500−4000 $cm^{-1}$ with a resolution of 4 $cm^{-1}$. The atmospheric $H_2O$ and $CO_2$ were subtracted, and baseline was achieved before each scan.

***In Situ* Visualization of Surface Adherence under NP Stress.** The surface adherence property of *A. chroococcum*, *B. thuringiensis*, *P. mosselii*, and *S. meliloti* on a glass surface while growing under NP stress was evaluated at MIC of Ag-NPs and ZnO-NPs. Adherence was assayed both qualitatively on glass cover slips and quantitatively in polystyrene microtiter well plates using the crystal violet (CV) staining method. A total of six polystyrene plates were filled with nutrient media amended with MIC concentration of both NPs followed by inoculation with young bacterial cultures ($1 \times 10^7$ CFU $mL^{-1}$) at a 1% inoculum rate. A glass coverslip in each well was then positioned at an approximate angle of 45°. The plates were incubated at 28 °C for 48 h for *B. thuringiensis*, *P. mosselii*, and *S. meliloti*, while *A. chroococcum* was incubated for 4 days under static conditions. After incubation, growth was removed gently from the wells and bacterial population adhered to glass coverslips were gently rinsed thrice with sterile PBS (1×). Coverslips were stained by 0.1% CV in double-distilled water (DDW), and images were captured by the use of an optical


https://dx.doi.org/10.1021/acsomega.9b04084
ACS Omega 2020, 5, 7861−7876

Olympus trinocular microscope (BX60; Japan) equipped with an Exwave HAD color video camera (Sony, Japan). For quantitative analysis, 100 $\mu$L of young cultures ($1 \times 10^7$ CFU $mL^{-1}$) were added to microtiter wells filled with respective nutrient broth. The mixture was then amended with the MIC concentration of Ag-NPs and ZnO-NPs. The bacterial cultures were incubated at 28 °C for appropriate time intervals. Controls were run in parallel. After incubation, wells were evacuated and washed with PBS. Staining with 0.1% crystal violet was performed and allowed to incubate for 30 min at 28 °C. The wells were again washed with PBS (1×), and crystal violet (CV) retained by the bacterial population was solubilized by adding 200 $\mu$L of 90% ethanol. The absorbance was recorded at 620 nm using a microplate reader.

**Bacterial Growth Curve under NP Stress.** Time- and concentration-dependent effects of Ag-NPs and ZnO-NPs were assessed by growing *A. chroococcum*, *B. thuringiensis*, *P. mosselii*, and *S. meliloti* in 96-well microtiter plates. Microtiter wells were filled with 200 $\mu$L of culture broth supplemented with 125, 250, 500, and 1000 $\mu$g $mL^{-1}$ of each NPs. The amended broths were inoculated with bacterial cultures ($1 \times 10^7$ CFU $mL^{-1}$) at a 1% inoculum rate. The control for each strain without NPs was included. Negative controls containing only NPs were also run, and the absorbance was subtracted from the wells inoculated with bacterial culture to avoid the fluctuations produced by reflectance of incident light by NPs. There were altogether three treatments: (i) bacterial cultures (independently) + individual concentration of each NPs, (ii) only individual bacterial cultures, and (iii) only NPs in broth. All treatments were replicated three times (Table S6). All plates were incubated at 28 °C overtime, and absorbance was recorded at 620 nm at regular intervals of 4 up to 16 h. Absorbance values of three independent replicates for each concentration was pooled together, and the mean value for each independent concentration and NPs was computed.

**Bacterial Cell Death Measured by CLSM.** Fluorescence detection of EPS and cell viability of *A. chroococcum*, *B. thuringiensis*, *P. mosselii*, and *S. meliloti* were examined under NP stress through CLSM. Bacterial cultures were grown on glass cover slips, as described previously (Section 2.9). Additionally, 5% of sucrose was added to the nutrient broth before growing cells. After 24 h, the coverslips were rinsed gently at least thrice with sterile PBS and staining was performed with 50 $\mu$M PI for 10 min at RT while keeping the coverslips in wells. After rinsing with PBS, cells were incubated with 50 $\mu$g $mL^{-1}$ concanavalin-A-conjugated fluorescein isothiocyanate (ConA-FITC; Sigma-Aldrich, USA) for 15 min at RT to stain the glycocalyx matrix green. The PI was excited at 535 nm, and the emission was recorded using a CLS microscope. Likewise, the ConA-FITC was excited at 495 nm and emission was recorded at 520 nm. Intact biofilms were examined nondestructively using a Leica TCS SPE, CLSM (Leica Microsystems, Germany) with Leica oil immersion lens.

**Generation of Superoxide by Bacterial Cells under NP Stress.** A quantitative assay was employed to determine the generation of superoxide anions by bacterial cells grown with 62.5−1000 $\mu$g $mL^{-1}$ NPs. Cells of *A. chroococcum*, *B. thuringiensis*, *P. mosselii*, and *S. meliloti* grown in respective growth media were separated as described for cellular respiration experiments (Section 2.5). Cell suspensions in PBS (1×) were incubated at 28 °C for 12 h with and without varying concentrations of Ag-NPs and ZnO-NPs. After treatment, NBT was added to cell suspensions maintaining the final concentration of NBT to be 1 mM and incubated for 20 min at RT. The release of super oxide anions ($O_2^{\cdot-}$) as deposits of blue color formazan was determined by measuring the absorbance of cell suspensions at 520 nm. Data was plotted as a function of NP concentration.

**Production of IAA under NP Stress.** The production of IAA by bacterial cultures was assessed by the modified method of ref 73 In brief, 100 $\mu$L of overnight grown *A. chroococcum*, *P. mosselii*, and *S. meliloti* culture was inoculated in LB broth (25 mL) supplemented with 100 $\mu$g $mL^{-1}$ tryptophan, and 62.5, 125, 250, 500, and 1000 $\mu$g $mL^{-1}$ each of Ag-NPs and ZnO-NPs. The control and treated cells were incubated at 28 °C at 100 r/min shaking. After a 48 h incubation, 2 mL of the culture from control and each treatment was centrifuged at 10,000 r/min for 10 min. The resulting supernatant was mixed with two or three drops of orthophosphoric acid ($H_3PO_4$) and 4 mL of the Salkowsky reagent (2% 0.5 M $FeCl_3$ in 35% $HClO_4$). Samples were incubated in the dark for 1 h. The IAA in the supernatant was quantified by measuring the absorbance of pink color using a spectrophotometer ($\lambda$ = 530 nm) against a standard curve of pure IAA.

**Statistical Analysis.** Data was analyzed by one-way analysis of variance (ANOVA), and the least significant difference (LSD) was calculated at a 5% probability level. The difference among treatment means was compared using Duncan's multiple range test (DMRT) at a 5% probability level. The data in the figures is represented as mean ± SD ($n$ = 3) for each measured parameter.

## ■ ASSOCIATED CONTENT

### Supporting Information

The Supporting Information is available free of charge at https://pubs.acs.org/doi/10.1021/acsomega.9b04084.

Details of bacterial cultures, FTIR bond assignments, cell viability images, TEM micrographs of bacterial cells with NPs attached to them, CLSM images of dual stained biofilm, growth curves, and NBT staining of bacterial cells (PDF)

## ■ AUTHOR INFORMATION


### Corresponding Author

**Bilal Ahmed** − *Department of Agricultural Microbiology, Aligarh Muslim University, Aligarh 202002, India;* orcid.org/0000-0001-8047-9231; Email: bilalahmed.amu@gmail.com

### Authors

**Fuad Ameen** − *Department of Botany and Microbiology, College of Science, King Saud University, Riyadh 11451, Saudi Arabia*

**Asfa Rizvi** − *Department of Agricultural Microbiology, Aligarh Muslim University, Aligarh 202002, India*

**Khursheed Ali** − *Department of Agricultural Microbiology, Aligarh Muslim University, Aligarh 202002, India*

**Hana Sonbol** − *Department of Biology, College of Science, Princess Nourah bint Abdulrahman University, Riyadh 11671, Saudi Arabia*

**Almas Zaidi** − *Department of Agricultural Microbiology, Aligarh Muslim University, Aligarh 202002, India*

**Mohammad Saghir Khan** − *Department of Agricultural Microbiology, Aligarh Muslim University, Aligarh 202002, India*




https://dx.doi.org/10.1021/acsomega.9b04084
ACS Omega 2020, 5, 7861−7876

**Javed Musarrat** − *Department of Agricultural Microbiology, Aligarh Muslim University, Aligarh 202002, India; School of Biosciences and Biotechnology, Baba Ghulam Shah Badshah University, Rajouri, Jammu and Kashmir 185234, India*

Complete contact information is available at: https://pubs.acs.org/10.1021/acsomega.9b04084

### Notes

The authors declare no competing financial interest.

## ■ ACKNOWLEDGMENTS

The research was funded by the Deanship of Scientific Research at Princess Nourah bint Abdulrahman University through the fast-track research funding group (Riyadh, Saudi Arabia). The authors are also thankful to the Department of Agricultural Microbiology, the Instrumentation Facility, the Department of Chemistry, the University Sophisticated Instrument Facility (USIF) at Aligarh Muslim University (Aligarh, India), Institute Instrumentation Center, Indian Institute of Technology (Roorkee, India), and the Electron Microscopy Facility, AIIMS (New Delhi, India) for providing research facilities for respective analysis.

## ■ REFERENCES

(1) Arakha, M.; Jha, S. Nanoparticle. In *Interfacial Phenomena on Biological Membranes. Series in BioEngineering*; Springer, Cham, 2018, pp 1−36.

(2) Barhoum, A.; Rahier, H.; Benelmekki, M.; Van Assche, G. Recent Trends in Nanostructured Particles: Synthesis, Functionalization, and Applications. In *Fundamentals of Nanoparticles*; Elsevier, 2018; pp 605−639.

(3) Ocsoy, I.; Paret, M. L.; Ocsoy, M. A.; Kunwar, S.; Chen, T.; You, M.; Tan, W. Nanotechnology in Plant Disease Management: DNA-Directed Silver Nanoparticles on Graphene Oxide as an Antibacterial against *Xanthomonas perforans*. *ACS Nano* **2013**, *7*, 8972−8980.

(4) Vittori Antisari, L.; Carbone, S.; Gatti, A.; Vianello, G.; Nannipieri, P. Uptake and Translocation of Metals and Nutrients in Tomato Grown in Soil Polluted with Metal Oxide ($CeO_2$, $Fe_3O_4$, $SnO_2$, $TiO_2$) or Metallic (Ag, Co, Ni) Engineered Nanoparticles. *Environ. Sci. Pollut. Res.* **2015**, *22*, 1841−1853.

(5) Rizwan, M.; Ali, S.; Qayyum, M. F.; Ok, Y. S.; Adrees, M.; Ibrahim, M.; Zia-ur-Rehman, M.; Farid, M.; Abbas, F. Effect of Metal and Metal Oxide Nanoparticles on Growth and Physiology of Globally Important Food Crops: A Critical Review. *J. Hazard. Mater.* **2017**, *322*, 2−16.

(6) Eduok, S.; Hendry, C.; Ferguson, R.; Martin, B.; Villa, R.; Jefferson, B.; Coulon, F. Insights into the Effect of Mixed Engineered Nanoparticles on Activated Sludge Performance. *FEMS Microbiol. Ecol.* **2015**, *91*, fiv082.

(7) Brown, J. Impact of Silver Nanoparticles on Wastewater Treatment. In *Nanotechnologies for Environmental Remediation: Applications and Implications*; Springer Cham., 2017; pp 255−267.

(8) Rajput, V. D.; Minkina, T.; Sushkova, S.; Tsitsuashvili, V.; Mandzhieva, S.; Gorovtsov, A.; Nevidomskyaya, D.; Gromakova, N. Effect of Nanoparticles on Crops and Soil Microbial Communities. *J. Soils Sediments* **2018**, *18*, 2179−2187.

(9) Dumont, E.; Johnson, A. C.; Keller, V. D. J.; Williams, R. J. Nano Silver and Nano Zinc-Oxide in Surface Waters − Exposure Estimation for Europe at High Spatial and Temporal Resolution. *Environ. Pollut.* **2015**, *196*, 341−349.

(10) Levard, C.; Hotze, E. M.; Lowry, G. V.; Brown, G. E., Jr. Environmental Transformations of Silver Nanoparticles: Impact on Stability and Toxicity. *Environ. Sci. Technol.* **2012**, *46*, 6900−6914.

(11) Seabra, A.; Durán, N. Nanotoxicology of Metal Oxide Nanoparticles. *Metals* **2015**, *5*, 934−975.

(12) Nowack, B. Environmental Behavior and Effects of Engineered Metal and Metal Oxide Nanoparticles. In *Handbook of Advanced Industrial and Hazardous Wastes Management*; Taylor & Francis, 2017; pp 905−929..

(13) Hong, J.; Rico, C. M.; Zhao, L.; Adeleye, A. S.; Keller, A. A.; Peralta-Videa, J. R.; Gardea-Torresdey, J. L. Toxic Effects of Copper-Based Nanoparticles or Compounds to Lettuce (*Lactuca Sativa*) and Alfalfa (*Medicago Sativa*). *Environ. Sci. Process. Impacts* **2015**, *17*, 177−185.

(14) Pittol, M.; Tomacheski, D.; Simões, D. N.; Ribeiro, V. F.; Santana, R. M. C. Macroscopic Effects of Silver Nanoparticles and Titanium Dioxide on Edible Plant Growth. *Environ. Nanotechnol., Monit. Manag.* **2017**, *8*, 127−133.

(15) Fayiga, A. O.; Saha, U. K. Nanoparticles in Biosolids: Effect on Soil Health and Crop Growth. *Peertechz J Environ. Sci Toxicol* **2017**, *2*, 59−67.

(16) Tripathi, D. K.; Shweta; Singh, S.; Singh, S.; Pandey, R.; Singh, V. P.; Sharma, N. C.; Prasad, S. M.; Dubey, N. K.; Chauhan, D. K. An Overview on Manufactured Nanoparticles in Plants: Uptake, Translocation, Accumulation and Phytotoxicity. *Plant Physiol. Biochem.* **2017**, *110*, 2−12.

(17) Saccá, M. L.; Barra Caracciolo, A.; Di Lenola, M.; Grenni, P. Ecosystem Services Provided By Soil Microorganisms. In *Soil Biological Communities and Ecosystem Resilience; Sustainability in Plant and Crop Protection*; Springer Cham., 2017; pp 9−24.

(18) Magheshwaran, V.; Govindasamy, V.; Annapurna, K.; Senthilkumar, M.; Sharma, V.; Bose, P.; Kumar, U. *Bacillus and Paenibacillus* Spp.: Potential PGPR for Sustainable Agriculture; In *Plant Growth and Health Promoting Bacteria. Microbiology Monographs*; Springer: Berlin, Heidelberg, 2010; pp 333−364.

(19) Etesami, H.; Maheshwari, D. K. Use of Plant Growth Promoting Rhizobacteria (PGPRs) with Multiple Plant Growth Promoting Traits in Stress Agriculture: Action Mechanisms and Future Prospects. *Ecotoxicol. Environ. Saf.* **2018**, 225−246.

(20) Zhang, L.; Wu, L.; Si, Y.; Shu, K. Size-Dependent Cytotoxicity of Silver Nanoparticles to *Azotobacter Vinelandii*: Growth Inhibition, Cell Injury, Oxidative Stress and Internalization. *PLoS One* **2018**, *13*, No. e0209020.

(21) Fukui, H.; Horie, M.; Endoh, S.; Kato, H.; Fujita, K.; Nishio, K.; Komaba, L. K.; Maru, J.; Miyauhi, A.; Nakamura, A.; et al. Association of Zinc Ion Release and Oxidative Stress Induced by Intratracheal Instillation of ZnO Nanoparticles to Rat Lung. *Chem.-Biol. Interact.* **2012**, *198*, 29−37.

(22) Wang, L.; Hu, C.; Shao, L. The Antimicrobial Activity of Nanoparticles: Present Situation and Prospects for the Future. *Int. J. Nanomed.* **2017**, *Volume 12*, 1227−1249.

(23) Mesa-Marín, J.; Del-Saz, N. F.; Rodríguez-Llorente, I. D.; Redondo-Gómez, S.; Pajuelo, E.; Ribas-Carbó, M.; Mateos-Naranjo, E. PGPR Reduce Root Respiration and Oxidative Stress Enhancing *Spartina maritima* Root Growth and Heavy Metal Rhizoaccumulation. *Front. Plant Sci.* **2018**, DOI: 10.3389/fpls.2018.01500.

(24) Yavuz, C. T.; Mayo, J. T.; Yu, W. W.; Prakash, A.; Falkner, J. C.; Yean, S.; Cong, L.; Shipley, H. J.; Kan, A.; Tomson, M.; et al. Low-Field Magnetic Separation of Monodisperse $Fe_3O_4$ nanocrystals. *Science* **2006**, *314*, 964−967.

(25) Mueller, N. C.; Nowack, B. Nanoparticles for Remediation: Solving Big Problems with Little Particles. *Elements* **2010**, *6*, 395−400.

(26) Cullen, L. G.; Tilston, E. L.; Mitchell, G. R.; Collins, C. D.; Shaw, L. J. Assessing the Impact of Nano- and Micro-Scale Zerovalent Iron Particles on Soil Microbial Activities: Particle Reactivity Interferes with Assay Conditions and Interpretation of Genuine Microbial Effects. *Chemosphere* **2011**, *82*, 1675−1682.

(27) Chen, Y.; Chao, Y.; Li, Y.; Lin, Q.; Bai, J.; Tang, L.; Wang, S.; Ying, R.; Qiu, R. Survival Strategies of the Plant-Associated Bacterium *Enterobacter Sp.* Strain EG16 under Cadmium Stress. *Appl. Environ. Microbiol.* **2016**, *82*, 1734−1744.

(28) Erdem, A.; Metzler, D.; Cha, D. K.; Huang, C. P. The Short-Term Toxic Effects of $TiO_2$ nanoparticles toward Bacteria through

Viability, Cellular Respiration, and Lipid Peroxidation. *Environ. Sci. Pollut. Res.* **2015**, *22*, 17917−17924.
(29) Shi, T.; Sun, X.; He, Q.-Y. Cytotoxicity of Silver Nanoparticles against Bacteria and Tumor Cells. *Curr. Protein Pept. Sci.* **2018**, *19*, 525−536.
(30) Ayangbenro, A.; Babalola, O. A New Strategy for Heavy Metal Polluted Environments: A Review of Microbial Biosorbents. *Int. J. Environ. Res. Public Health* **2017**, *14*, 94.
(31) Wagner, G.; Korenkov, V.; Judy, J.; Bertsch, P. Nanoparticles Composed of Zn and ZnO Inhibit *Peronospora Tabacina* Spore Germination *in Vitro* and *P. tabacina* Infectivity on Tobacco Leaves. *Nanomaterials* **2016**, *6*, 50.
(32) Duhan, J. S.; Kumar, R.; Kumar, N.; Kaur, P.; Nehra, K.; Duhan, S. Nanotechnology: The New Perspective in Precision Agriculture. *Biotechnol. Rep.* **2017**, *15*, 11−23.
(33) Zaidi, A.; Khan, M. S.; Saif, S.; Rizvi, A.; Ahmed, B.; Shahid, M. Role of nitrogen-fixing plant growth-promoting rhizobacteria in sustainable production of vegetables: current perspective. In *Microbial Strategies for Vegetable Production*; Zaidi, A., Khan, M. S., Eds.; Springer, Cham., 2017, 49−79.
(34) Kaweeteerawat, C.; Ivask, A.; Liu, R.; Zhang, H.; Chang, C. H.; Low-Kam, C.; Fischer, H.; Ji, Z.; Pokhrel, S.; Cohen, Y.; et al. Toxicity of Metal Oxide Nanoparticles in *Escherichia Coli* Correlates with Conduction Band and Hydration Energies. *Environ. Sci. Technol.* **2015**, *49*, 1105−1112.
(35) Piotrowska-Seget, Z.; Cycoń, M.; Kozdrój, J. Metal-Tolerant Bacteria Occurring in Heavily Polluted Soil and Mine Spoil. *Appl. Soil Ecol.* **2005**, *28*, 237−246.
(36) Niño-Martínez, N.; Salas Orozco, M. F.; Martínez-Castañón, G. A.; Torres Méndez, F.; Ruiz, F. Molecular Mechanisms of Bacterial Resistance to Metal and Metal Oxide Nanoparticles. *International journal of molecular sciences.* **2019**, *20*, 2808.
(37) Asadishad, B.; Chahal, S.; Akbari, A.; Cianciarelli, V.; Azodi, M.; Ghoshal, S.; Tufenkji, N. Amendment of Agricultural Soil with Metal Nanoparticles: Effects on Soil Enzyme Activity and Microbial Community Composition. *Environ. Sci. Technol.* **2018**, *52*, 1908−1918.
(38) Sedlak, R. H.; Hnilova, M.; Grosh, C.; Fong, H.; Baneyx, F.; Schwartz, D.; Sarikaya, M.; Tamerler, C.; Traxler, B. Engineered *Escherichia Coli* Silver-Binding Periplasmic Protein That Promotes Silver Tolerance. *Appl. Environ. Microbiol.* **2012**, *78*, 2289−2296.
(39) Helmann, J. D.; Moran, C. P. RNA Polymerase; Sigma Factors. In *Bacillus subtilis and Its Closest Relatives*; 2014; pp 289−312.
(40) Feng, Q. L.; Wu, J.; Chen, G. Q.; Cui, F. Z.; Kim, T. N.; Kim, J. O. A Mechanistic Study of the Antibacterial Effect of Silver Ions on *Escherichia Coli* and Staphylococcus Aureus. *J. Biomed. Mater. Res.* **2000**, *52*, 662−668.
(41) Jung, W. K.; Koo, H. C.; Kim, K. W.; Shin, S.; Kim, S. H.; Park, Y. H. Antibacterial Activity and Mechanism of Action of the Silver Ion in *Staphylococcus aureus* and *Escherichia Coli*. *Appl. Environ. Microbiol.* **2008**, *74*, 2171−2178.
(42) Horie, M.; Stowe, M.; Tabei, M.; Kuroda, E. Metal Ion Release of Manufactured Metal Oxide Nanoparticles Is Involved in the Allergic Response to Inhaled Ovalbumin in Mice. *Occup. Dis. Environ. Med.* **2016**, *04*, 17−26.
(43) Tripathi, D. K.; Tripathi, A.; Shweta; Singh, S.; Singh, Y.; Vishwakarma, K.; Yadav, G.; Sharma, S.; Singh, V. K.; Mishra, R. K.; et al. Uptake, Accumulation and Toxicity of Silver Nanoparticle in Autotrophic Plants, and Heterotrophic Microbes: A Concentric Review. *Front. Microbiol.* **2017**, DOI: 10.3389/fmicb.2017.00007.
(44) McGivney, E.; Han, L.; Avellan, A.; Vanbriesen, J.; Gregory, K. B. Disruption of Autolysis in *Bacillus subtilis* Using $TiO_2$ Nanoparticles. *Sci. Rep.* **2017**, *7*, 44308.
(45) Wahab, R.; Khan, S. T.; Dwivedi, S.; Ahamed, M.; Musarrat, J.; Al-Khedhairy, A. A. Effective Inhibition of Bacterial Respiration and Growth by CuO Microspheres Composed of Thin Nanosheets. *Colloids Surf., B* **2013**, *111*, 211−217.
(46) Choi, O.; Deng, K. K.; Kim, N.-J.; Ross, L., Jr.; Surampalli, R. Y.; Hu, Z. The Inhibitory Effects of Silver Nanoparticles, Silver Ions, and Silver Chloride Colloids on Microbial Growth. *Water Res.* **2008**, *42*, 3066−3074.
(47) Gambino, M.; Marzano, V.; Villa, F.; Vitali, A.; Vannini, C.; Landini, P.; Cappitelli, F. Effects of Sublethal Doses of Silver Nanoparticles on *Bacillus subtilis* Planktonic and Sessile Cells. *J. Appl. Microbiol.* **2015**, *118*, 1103−1115.
(48) Rizvi, A.; Zaidi, A.; Khan, M. S.; Saif, S.; Ahmed, B.; Shahid, M. Growth improvement and management of vegetable diseases by plant growth-promoting rhizobacteria. In *Microbial Strategies for Vegetable Production*; Zaidi, A., Khan, M. S., Eds.; Springer, Cham., 2017, 99−123.
(49) Rizvi, A.; Ahmed, B.; Zaidi, A.; Khan, M. S. Bioreduction of Toxicity Influenced by Bioactive Molecules Secreted under Metal Stress by *Azotobacter chroococcum*. *Ecotoxicology* **2019**, *28*, 302−322.
(50) Enders, T. A.; Strader, L. C. Auxin Activity: Past, Present, and Future. *Am. J. Bot.* **2015**, *102*, 180−196.
(51) Seneviratne, M.; Gunaratne, S.; Bandara, T.; Weerasundara, L.; Rajakaruna, N.; Seneviratne, G.; Vithanage, M. Plant Growth Promotion by *Bradyrhizobium japonicum* under Heavy Metal Stress. *S. Afr. J. Bot.* **2016**, *105*, 19−24.
(52) Yang, Y.; Wang, J.; Zhu, H.; Colvin, V. L.; Alvarez, P. J. Relative Susceptibility and Transcriptional Response of Nitrogen Cycling Bacteria to Quantum Dots. *Environ. Sci. Technol.* **2012**, *46*, 3433−3441.
(53) Yang, Y.; Wang, J.; Xiu, Z.; Alvarez, P. J. J. Impacts of Silver Nanoparticles on Cellular and Transcriptional Activity of Nitrogen-Cycling Bacteria. *Environ. Toxicol. Chem.* **2013**, *32*, 1488−1494.
(54) Golding, C. G.; Lamboo, L. L.; Beniac, D. R.; Booth, T. F. The Scanning Electron Microscope in Microbiology and Diagnosis of Infectious Disease. *Sci. Rep.* **2016**, *6*, 26516.
(55) Dufrêne, Y. F. Atomic Force Microscopy in Microbiology: New Structural and Functional Insights into the Microbial Cell Surface. *MBio* **2014**, *5*, No. e01363.
(56) Haris, Z.; Ahmad, I. Impact of Metal Oxide Nanoparticles on Beneficial Soil Microorganisms and Their Secondary Metabolites. *Int. J. Life-Sciences Sci. Res.* **2017**, *3*, 1020.
(57) Diaz-Visurraga, J.; Cardenas, G.; Garcia, A. Morphological Changes Induced in Bacteria as Evaluated by Electron Microscopy. *Microsc. Sci. Technol. Appl. Educ.* **2010**, 307−315.
(58) Sun, D.; Zhang, W.; Li, N.; Zhao, Z.; Mou, Z.; Yang, E.; Wang, W. Silver Nanoparticles-Quercetin Conjugation to SiRNA against Drug-Resistant *Bacillus subtilis* for Effective Gene Silencing: In Vitro and in Vivo. *Mater. Sci. Eng. C* **2016**, *63*, 522−534.
(59) Lubitz, P.; Mayr, U. B.; Lubitz, W. Applications of Bacterial Ghosts in Biomedicine. *Adv. Exp. Med. Biol.* **2009**, *655*, 159−170.
(60) Verma, S. K.; Jha, E.; Sahoo, B.; Panda, P. K.; Thirumurugan, A.; Parashar, S. K. S.; Suar, M. Mechanistic Insight into the Rapid One-Step Facile Biofabrication of Antibacterial Silver Nanoparticles from Bacterial Release and Their Biogenicity and Concentration-Dependent in Vitro Cytotoxicity to Colon Cells. *RSC Adv.* **2017**, *7*, 40034−40045.
(61) Oz, Y.; Abdouni, Y.; Yilmaz, G.; Becer, C. R.; Sanyal, A. Magnetic Glyconanoparticles for Selective Lectin Separation and Purification. *Polym. Chem.* **2019**, *10*, 3351−3361.
(62) Hussain, H.; L, S. R.; Ahmad, S.; Abd. Razak, M. F.; Wan Mohamud, W. N.; Bakar, J.; Ghazali, H. M. Determination of Cell Viability Using Acridine Orange/Propidium Iodide Dual-Spectro-fluorometry Assay. *Cogent Food Agric.* **2019**, *5*, 1582398.
(63) Gupta, P.; Diwan, B. Bacterial Exopolysaccharide Mediated Heavy Metal Removal: A Review on Biosynthesis Mechanism and Remediation Strategies. *Biotechnol. Rep.* **2017**, *13*, 58−71.
(64) Taylor, C.; Matzke, M.; Kroll, A.; Read, D. S.; Svendsen, C.; Crossley, A. Toxic Interactions of Different Silver Forms with Freshwater Green Algae and Cyanobacteria and Their Effects on Mechanistic Endpoints and the Production of Extracellular Polymeric Substances. *Environ. Sci. Nano* **2016**, *3*, 396−408.
(65) Khan, S. T.; Ahmad, J.; Ahamed, M.; Musarrat, J.; Al-Khedhairy, A. A. Zinc Oxide and Titanium Dioxide Nanoparticles Induce Oxidative Stress, Inhibit Growth, and Attenuate Biofilm

Formation Activity of *Streptococcus mitis*. *J. Biol. Inorg. Chem.* **2016**, *21*, 295−303.
(66) Bondarenko, O. M.; Sihtmäe, M.; Kuzmičiova, J.; Ragelienė, L.; Kahru, A.; Daugelavičius, R. Plasma Membrane Is the Target of Rapid Antibacterial Action of Silver Nanoparticles in *Escherichia coli* and *Pseudomonas aeruginosa*. *Int. J. Nanomed.* **2018**, *Volume 13*, 6779−6790.
(67) Slavin, Y. N.; Asnis, J.; Häfeli, U. O.; Bach, H. Metal Nanoparticles: Understanding the Mechanisms behind Antibacterial Activity. *J. Nanobiotechnol.* **2017**, *15*, 65.
(68) Vishnupriya, S.; Chaudhari, K.; Jagannathan, R.; Pradeep, T. Single-Cell Investigations of Silver Nanoparticle-Bacteria Interactions. *Part. Part. Syst. Charact.* **2013**, *30*, 1056−1062.
(69) Dimkpa, C. O.; Calder, A.; Britt, D. W.; McLean, J. E.; Anderson, A. J. Responses of a Soil Bacterium, *Pseudomonas chlororaphis* O6 to Commercial Metal Oxide Nanoparticles Compared with Responses to Metal Ions. *Environ. Pollut.* **2011**, *159*, 1749−1756.
(70) Ahmed, B.; Rizvi, A.; Zaidi, A.; Khan, M. S.; Musarrat, J. Understanding the Phyto-Interaction of Heavy Metal Oxide Bulk and Nanoparticles: Evaluation of Seed Germination, Growth, Bioaccumulation, and Metallothionein Production. *RSC Adv.* **2019**, *9*, 4210−4225.
(71) Ahmed, B.; Hashmi, A.; Khan, M. S.; Musarrat, J. ROS Mediated Destruction of Cell Membrane, Growth and Biofilms of Human Bacterial Pathogens by Stable Metallic AgNPs Functionalized from Bell Pepper Extract and Quercetin. *Adv. Powder Technol.* **2018**, *29*, 1601−1616.
(72) Shakeri, S.; Kermanshahi, R. K.; Moghaddam, M. M.; Emtiazi, G. Assessment of Biofilm Cell Removal and Killing and Biocide Efficacy Using the Microtiter Plate Test. *Biofouling* **2007**, *23*, 79−86.
(73) Bric, J. M.; Bostock, R. M.; Silverstone, S. E. Rapid in Situ Assay for Indoleacetic Acid Production by Bacteria Immobilized on a Nitrocellulose Membrane. *Appl. Environ. Microbiol.* **1991**, *57*, 535−538.


https://dx.doi.org/10.1021/acsomega.9b04084
*ACS Omega* 2020, 5, 7861−7876